

1 **Synergetic effects of NH<sub>3</sub> and NO<sub>x</sub> on the production**  
2 **and optical absorption of secondary organic aerosol**  
3 **formation from toluene photooxidation**

4

5

6

7

8 Shijie Liu <sup>a</sup>, Dandan Huang <sup>b</sup>, Yiqian Wang <sup>a</sup>, Si Zhang <sup>a</sup>, Can Wu, Wei Du, Gehui  
9 Wang <sup>a,c,\*</sup>

10

11

12 <sup>a</sup> Key Lab of Geographic Information Science of the Ministry of Education, School of  
13 Geographic Sciences, East China Normal University, Shanghai 210062, China

14 <sup>b</sup> State Environmental Protection Key Laboratory of Formation and Prevention of the  
15 Urban Air Pollution Complex, Shanghai Academy of Environmental Sciences,  
16 Shanghai 200233, China

17 <sup>c</sup> Institute of Eco-Chongming, Cuiniao Road, Chengjia Zheng, Shanghai 202150, China.

18

19

20 Corresponding author: Prof. Gehui Wang, e-mail: [ghwang@geo.ecnu.edu.cn](mailto:ghwang@geo.ecnu.edu.cn)

21

## 22 **Abstract**

23  $\text{NH}_3$  is the most important alkaline gas in the atmosphere and one of the key  
24 species affecting the behaviors of atmospheric aerosols. However, the impact of  $\text{NH}_3$   
25 on secondary organic aerosol (SOA) formation remains poorly understood, especially  
26 the dynamic evolution of chemical compositions in the SOA formation process. A series  
27 of chamber experiments was performed to probe the individual and common effects of  
28  $\text{NH}_3$  and  $\text{NO}_x$  on toluene SOA formation through OH-photooxidation. The chemical  
29 compositions of toluene SOA were characterized using the Aerodyne high-resolution  
30 time-of-flight aerosol mass spectrometer (AMS). From  $637 \pm 14.6 \mu\text{g m}^{-3}$  (control), the  
31 SOA mass concentration increased to  $867 \pm 12.7 \mu\text{g m}^{-3}$  in the presence of  $\text{NH}_3$  and  
32 decreased to  $452 \pm 18.9 \mu\text{g m}^{-3}$  in the presence of  $\text{NO}_x$ . However, the highest SOA  
33 concentration ( $1020 \pm 10.6 \mu\text{g m}^{-3}$ ) and the lowest carbon oxidation state ( $\text{OS}_C$ )  
34 occurred in the presence of both  $\text{NH}_3$  and  $\text{NO}_x$ , indicating that the higher volatility  
35 products that formed in the presence of  $\text{NO}_x$  could precipitate into the particle-phase  
36 when  $\text{NH}_3$  was added. This resulted in a synergetic effect on SOA formation when  $\text{NH}_3$   
37 and  $\text{NO}_x$  co-existed. The heterogeneous reaction was the main pathway by which  $\text{NH}_3$   
38 participated in SOA formation in the photooxidation process. The synergetic effect of  
39  $\text{NH}_3$  and  $\text{NO}_x$  was also observed in SOA optical absorption. A peak at 280 nm, which  
40 is characteristic of organonitrogen imidazole compounds, was observed in the presence  
41 of  $\text{NH}_3$  and its intensity increased when  $\text{NO}_x$  was added into the chamber. This work  
42 improves our understanding of how the synergistic interactions between  $\text{NH}_3$  and  $\text{NO}_x$   
43 influence SOA formation and offers new insights into mitigating haze pollution.

44 **Keywords:** Photooxidation; Toluene; NH<sub>3</sub>; Dynamic characteristics; Synergistic

45 effects

46

## 47 **1 Introduction**

48 Secondary organic aerosols (SOA) are an important component of atmospheric  
49 particulate matter (Moise et al., 2015;Liu et al., 2017). SOA can significantly affect  
50 atmospheric visibility, air quality, and subsequently public health (Paciga et al.,  
51 2014;Yang et al., 2016;Liu et al., 2017). The optical properties of SOA have been  
52 directly and indirectly linked to their effects on the climate (Laskin et al., 2015;Xie et  
53 al., 2017;Peng et al., 2020). Because of the complexity of their chemical components,  
54 oxidation processes, and environmental factors, SOA formation mechanisms are very  
55 complex and the current understanding of SOA formation is incomplete. This limited  
56 understanding hampers the ability of models to predict the magnitudes, dynamics, and  
57 distributions of atmospheric aerosols from particulate and precursor emissions (Ortiz-  
58 Montalvo et al., 2014). In the past decades, although our understanding of SOA  
59 formation mechanisms has been constantly improving, there is still a gap between the  
60 simulated SOA concentration in large-scale atmospheric models and field observations  
61 (Volkamer et al., 2006;Yang et al., 2018).

62 Ammonia (NH<sub>3</sub>) is the most important alkaline inorganic gas. It is widespread in  
63 the atmosphere and is one of the critical factors influencing SOA formation (Wang et  
64 al., 2016;Wang et al., 2018b;Chen et al., 2019). Some studies have noted that the  
65 presence of NH<sub>3</sub> can contribute to the formation of more aerosol mass through  
66 photooxidation (Na et al., 2007;Li et al., 2018). Na et al. (2007) observed that aerosol  
67 yields in the  $\alpha$ -pinene-ozone oxidation system increased by 8% when NH<sub>3</sub> was added.  
68 Li et al. (2018) concluded that the presence of NH<sub>3</sub> in the aromatic hydrocarbon

69 photooxidation system increased aerosol size growth potentials (by 7%–108%), and  
70 resulted in enhanced SOA formation. Qi et al. (2020) found that the concentration and  
71 average diameter of SOA showed an immediate and rapid increase after adding NH<sub>3</sub>.  
72 Furthermore, the acid-base reactions between NH<sub>3</sub>/NH<sub>4</sub><sup>+</sup> and the carboxyl groups in  
73 SOA molecules might enhance SOA formation (Qi et al., 2020;Liu et al., 2015). The  
74 condensable ammonium salts formed from the reaction between NH<sub>3</sub> and organic acids  
75 reduce the volatility of the organic acids by several orders of magnitude (Paciga et al.,  
76 2014), and act as particle-phase organics that further promote SOA formation (Na et al.,  
77 2007;Huang et al., 2012;Chen et al., 2019;Qi et al., 2020;Wu et al., 2020). Along  
78 another pathway, carbonyls can undergo nucleophilic attack by NH<sub>3</sub> through the  
79 Maillard reactions and form the corresponding iminium intermediates (Noziere et al.,  
80 2009;Laskin et al., 2015;Liu et al., 2015). The iminium intermediates can continue to  
81 react with carbonyls, which activates further transformations such as the formation of  
82 heterocyclic compounds and oligomerization reactions and forms condensation  
83 (oligomeric) products with more stable secondary imines (Schiff bases) (Laskin et al.,  
84 2014). Both Noziere et al. (2009) and Ortiz-Montalvo et al. (2014) reported NH<sub>3</sub> is an  
85 efficient catalyst for reactions with carbonyl compounds to form nitrogen-containing  
86 organic aerosols (NOA). The reaction between carbonyl and NH<sub>3</sub> can significantly  
87 decrease the volatility of oxidation products, which further increases the yield of SOA  
88 (Lee et al., 2013;Zhang et al., 2015a;Qi et al., 2020). Babar et al. (2017) found that the  
89 substantial formation of secondary imines in the presence of NH<sub>3</sub> was responsible for  
90 the higher  $\alpha$ -pinene SOA yields. However, not all studies have shown that the presence

91 of NH<sub>3</sub> increases SOA yields. One study observed that NH<sub>3</sub> suppressed SOA formation  
92 under certain ozonation conditions (Ma et al., 2018b). Furthermore, the consumption  
93 of NH<sub>3</sub> by Criegee intermediates was reported to decrease the secondary ozonide yield  
94 and thus affect SOA formation.

95 Nitrogen oxides (NO<sub>x</sub> = NO + NO<sub>2</sub>), which are mainly emitted from the  
96 combustion of fossil-fuels, have received significant attention due to their effects on the  
97 photooxidation process of volatile organic compounds (VOCs) and SOA formation  
98 (Surratt et al., 2006;Ng et al., 2007b;Draper et al., 2015;Berkemeier et al.,  
99 2016;Sarrafzadeh et al., 2016;Zhao et al., 2018). A clear increase at first and then a  
100 decrease in the SOA yield was found with increasing NO<sub>x</sub> concentration from the  
101 laboratory experiments with both artificial (trimethylbenzene) and biological (β-pinene)  
102 VOCs (Sarrafzadeh et al., 2016;Yang et al., 2020). The competitive chemistry of  
103 organic peroxy radicals (RO<sub>2</sub>) with hydroperoxy radicals (HO<sub>2</sub>) and NO was  
104 responsible for the variability in SOA formation (Ng et al., 2007a;Xu et al., 2014;Jiang  
105 et al., 2020). RO<sub>2</sub> mainly reacts with HO<sub>2</sub> under low-NO<sub>x</sub> conditions to form oxidation  
106 products with lower volatility, which may enable it to precipitate into the particle-phase  
107 and contribute to the SOA mass (Ng et al., 2007a). While the RO<sub>2</sub> + NO reaction is  
108 dominant in high-NO<sub>x</sub> conditions, the increase in volatile products formed through  
109 fragmentation was responsible for the decrease in SOA yield with increasing NO<sub>x</sub>  
110 (Zhao et al., 2018;Liu et al., 2019a;Xu et al., 2020). In addition, the increase of OH  
111 concentration formed through NO + HO<sub>2</sub> → NO<sub>2</sub> + OH reaction at low-NO<sub>x</sub> conditions,  
112 and a suppressing effect of NO<sub>x</sub> on OH formation under high-NO<sub>x</sub> conditions was

113 partly responsible for the first increasing and then decreasing trend of SOA yield with  
114 NO<sub>x</sub> concentration (Sarrafzadeh et al., 2016; Bates et al., 2021).

115 In the last decade, atmospheric pollutants in China have changed significantly in  
116 their concentrations and composition (Wang et al., 2015; Xia et al., 2016) with the  
117 emissions of SO<sub>2</sub> and NO<sub>x</sub> decreased by 75% from 2007–2015 and 10% from 2011–  
118 2015, respectively (de Foy et al., 2016; Vu et al., 2019; Wang et al., 2020). However,  
119 owing to the lack of regulation regarding NH<sub>3</sub> emissions, NH<sub>3</sub> emissions increased by  
120 ~30 % from 2008–2016 over the North China Plain (Liu et al., 2018). As has been  
121 pointed out in previous research, the promoting effect of NH<sub>3</sub> on the formation of SOA  
122 may counteract the decreases in aerosol formation due to reductions in SO<sub>2</sub> and NO<sub>x</sub>  
123 (Zhang et al., 2021a). Indeed, field observation and model simulation have pointed out  
124 that the reduction of NH<sub>3</sub> emissions contribute much to the improvement of PM<sub>2.5</sub>  
125 pollution compared to SO<sub>2</sub> in winter (Erisman and Schaap, 2004). Hence, the  
126 mechanism by which NH<sub>3</sub> affects SOA formation has attracted more and more attention  
127 (Wang et al., 2018a; Ge et al., 2019; Zhang et al., 2021b). However, previous studies  
128 have not paid sufficient attention to the joint impacts of NH<sub>3</sub> and NO<sub>x</sub> on the formation  
129 of SOA and its corresponding optical properties. Due to the lack of real time detection  
130 methods for SOA chemical composition, the dynamic characteristics of how NH<sub>3</sub>  
131 participates in SOA formation via photooxidation have not been extensively studied.

132 Toluene is one of the most abundant aromatic VOCs in the urban atmosphere,  
133 which is also an important source of brown carbon (Laskin et al., 2010; Ma et al., 2018a).  
134 The effects of NH<sub>3</sub> and NO<sub>x</sub> on SOA formation through the toluene photooxidation

135 process were investigated in this study. The chemical composition of toluene SOA was  
136 characterized on-line with an aerosol mass spectrometer and the characteristics of SOA  
137 chemical composition under different conditions were further explored by applying a  
138 positive matrix factorization (PMF) analysis. The optical properties of toluene SOA  
139 particles were determined based on a UV-vis spectrum analysis. Possible mechanisms  
140 of the effects of both NH<sub>3</sub> and NO<sub>x</sub> on SOA formation were discussed. The results will  
141 help us to better understand SOA formation mechanisms in complex pollution  
142 conditions with elevated NH<sub>3</sub> and NO<sub>x</sub> concentrations in an urban atmospheric  
143 environment.

## 144 **2 Materials and Methods**

### 145 **2.1 Photooxidation chamber experiments**

146 All toluene photooxidation experiments were performed in a 4 m<sup>3</sup> chamber. The  
147 chamber has been described in detail in our previous study (Liu et al., 2021). Briefly,  
148 the chamber was constructed with a 0.08 mm-thick FEP-Teflon film. 50 UV-B lamps  
149 (TUV36W, Philips) with peak wavelengths of 254 nm were set up around the chamber  
150 and used as the light source to drive OH radical formation through hydrogen peroxide  
151 (H<sub>2</sub>O<sub>2</sub>) photolysis. Mirror surfaced stainless steel was used as the interior wall of the  
152 enclosure to maximize and homogenize the interior light intensity. All experiments  
153 were performed at room temperature (293~298 K) and one atmospheric pressure was  
154 maintained in the chamber at all time.



155 Before each experiment, the chamber was flushed with zero air for at last 18 hours,  
156 after which the concentration of particles was less than  $1 \text{ cm}^{-3}$ . Zero air was generated  
157 by a zero air supply (111-D3N, Thermo Scientific<sup>TM</sup>, USA). The flow rate of zero air  
158 was controlled at  $20 \text{ L min}^{-1}$  by a mass flow controller (D088C/ZM, Beijing Sevenstar  
159 Electron Corporation) during the process of inflating. The relative humidity (RH) of  
160 zero air was about 20%. For each experiment, measured amounts of toluene (Sigma-  
161 Aldrich, analytically pure) and  $\text{H}_2\text{O}_2$  solution (Sigma-Aldrich, 30 wt% in  $\text{H}_2\text{O}$ ) were  
162 injected into a Teflon bulb with micro syringes. Zero air was passed through the  
163 injection tube to make sure all the liquids had evaporated to the gas-phase and were  
164 blown into the chamber. Toluene concentration was measured with a Proton Transfer  
165 Reaction-Mass Spectrometry (PTR-ToF-MS, Ionicon Analytik, Austria). The evolution  
166 of toluene concentration for different experiments was shown in Fig. S1. The OH  
167 concentration in the chamber was calculated based on the first order decay of toluene  
168 concentration. There was no obvious difference of OH concentrations in the different  
169  $\text{NO}_x$  and  $\text{NH}_3$  levels (Fig. S2). The average OH concentration over the entire reaction  
170 period was  $5.87 \times 10^7 \text{ molecule cm}^{-3}$ .  $\text{NO}_x$  (Air Liquid Shanghai, 510 ppm  $\text{NO}_2$  in  $\text{N}_2$ )  
171 and/or  $\text{NH}_3$  (Air Liquid Shanghai, 502 ppm  $\text{NH}_3$  in  $\text{N}_2$ ) were introduced directly into  
172 the chamber to reach the required concentrations. For experiments with  $\text{NO}_x$ , although  
173 only  $\text{NO}_2$  was introduced into the chamber before photooxidation, NO could be formed  
174 through  $\text{NO}_2$  photolysis under the UV light irradiation, so NO always coexisted with  
175  $\text{NO}_2$  in the photooxidation system (Zhao et al., 2018). Each experiment was performed  
176 without seed aerosols. After all the reactants were added, the chamber stood quietly for

177 10 min without turning on the light to ensure that the reactant gases in the chamber  
178 were evenly mixed. The photooxidation started when the UV light was turn on.

179 The experimental conditions for the toluene photooxidation are listed in Table 1.  
180 In our work, the OH and toluene concentrations were higher than those of urban  
181 conditions. The purpose of the high OH and toluene concentrations is to obtain enough  
182 particle production samples for off-line collections and accurate measurements. The  
183 toluene concentrations remained stable under the different experimental conditions, the  
184 variation of toluene-derived SOA mass concentration and yield was only affected by  
185 the different NO<sub>2</sub> and/or NH<sub>3</sub> concentrations in this study. Toluene was studied here as  
186 the representative of total aromatic VOCs in the urban atmosphere. The concentration  
187 ratio of toluene to OH in this study is similar to that under the real atmospheric  
188 conditions (Prinn et al., 1995;Zou et al., 2015).

## 189 **2.2 Particle concentration measurements**

190 For each experiment, a scanning mobility particle sizer (SMPS) was used to record  
191 the particle size distribution and volume concentration of the toluene-derived SOA. The  
192 SMPS was composed of a differential mobility analyzer (DMA model 3081, TSI Inc.,  
193 USA) and a condensation particle counter (CPC model 3776, TSI Inc., USA) which  
194 were used for screening particles with specific aerodynamic equivalent sizes (from 14.1  
195 nm to 736.5 nm) and for counting the number of the selected particles, respectively.  
196 The sheath gas velocity was 3 L min<sup>-1</sup> and the sample gas velocity was 0.3 L min<sup>-1</sup>. The  
197 scan was repeated every 5 min. During each scan circle, the scan time was 240 s, and

198 the particle sizes ranged from 13.6 nm to 726.5 nm. A density of  $1.4 \text{ g m}^{-3}$ , which was  
199 measured by Ng et al. (2007), was used for the calculation of toluene SOA mass  
200 concentration from the particle volume concentration (Ng et al., 2007b).

## 201 **2.3 Chemical characterization**

202 In this study, the toluene SOA chemical compositions were characterized with an  
203 on-line high-resolution time-of-flight aerosol mass spectrometer (HR-ToF-AMS,  
204 Aerodyne Research Inc. USA). The sample flow passed through a Nafion dryer and the  
205 RH of the sample gas was reduced to below 20% before entering the AMS. In the  
206 injection port, an aerodynamic lens focused particles with a vacuum aerodynamic  
207 diameter below  $1 \mu\text{m}$  into a narrow beam. Particles impacted a flash vaporizer ( $600^\circ\text{C}$ )  
208 at the rear of the sizing region under high vacuum ( $\sim 10^{-7}$  Torr) and were subsequently  
209 ionized by electron impact ionization (70 eV). Then, the positively charged ions entered  
210 the ToF section and were separated. V-mode ( $m/\Delta m = \sim 2000$ ) was used in the AMS  
211 ToF section to achieve the high signal-to-noise ratio. The separated ion fragments were  
212 analyzed by a mass spectrometer with scans from 1 to 300 m/z. The composition-  
213 dependent collection efficiency (CE) was applied to the data based on the methods  
214 established by Middlebrook et al. (2012). For mass concentration calculations, 1.1, 1.2,  
215 and 1.4 were applied as the default relative ionization efficiency (RIE) values of nitrate,  
216 sulfate, and organic compounds, respectively. The standard AMS data analysis software  
217 SQUIRREL 1.63B coupled with PIKA 1.23B in the Igor Pro (WaveMetrics, Inc.,  
218 Portland, Oregon), which were retrieved from <http://cires1.colorado.edu/jimenez->

219 [group/ToFAMSResources/ToFSoftware/](#), were used for the analysis of elemental ratios  
220 and the ion speciated compositions of toluene SOA in the chamber. Note that the  
221 elemental ratios (i.e., O/C, H/C, and N/C) and mass-to-carbon ratio (OM/OC) were all  
222 calculated using the Aiken-Ambient method for comparability with previous studies  
223 (Aiken et al., 2008). In order to further explore the changes in SOA chemical  
224 composition, a PMF of the high-resolution mass spectra was performed to determine  
225 the different organic aerosol (OA) factors during the toluene photooxidation process.  
226 We performed the PMF analysis in the same way as Zhang et al. (2011), the details of  
227 which are provided in the Supporting Information.

## 228 **2.4 Absorption measurements**

229 The changes of absorption spectra and the absorbance of the toluene derived SOA  
230 under different conditions were determined using a UV spectrophotometer (UV-3600,  
231 Shimadzu, Japan) with a 1 cm cuvette. The SOA was collected from a 3 m<sup>3</sup> sample gas  
232 onto the 46.2 nm PTFE filter (Whatman<sup>TM</sup>, UK). The collected SOA sample was  
233 dissolved in 5 mL of methanol (HPLC grade, > 99.8%) with 30 min of sonication. As  
234 reported by Chen and Bond (2010), > 92 % of SOA is extractable by organic solvents  
235 (e.g., methanol), which means that almost all organic matter was extracted in this study.  
236 The filter extracts were filtered through 0.2 μm PTFE syringe filters to remove  
237 suspended insoluble particles. Before detection of the optical absorbance, a cuvette  
238 filled with pure methanol was scanned as a blank to provide a spectral background. The  
239 absorption was detected over the range of 200 to 800 nm with a resolution of 0.5 nm<sup>-1</sup>.

240 The light absorption coefficient of the particles at a specific wavelength  $\lambda$  ( $Abs_{\lambda}$ , M/m)  
241 was calculated according to Eq. R1:

$$Abs_{\lambda} = (A_{\lambda} - A_{700}) \cdot \frac{V_1}{V_a \cdot L} \cdot \ln(10) \quad (R1)$$

242 where,  $A_{700}$  is the background value of light absorption intensity, calculated as the  
243 average value of light absorption intensity from 695–705 nm to reduce the limits of  
244 error in measurement;  $V_1$  and  $V_a$  are the volumes of methanol with dissolved particles  
245 and sampled air, respectively; and  $L$  is the optical path length. Because  $Abs_{\lambda}$  was  
246 strongly dependent on the amount of SOA, all  $Abs_{\lambda}$  results were normalized based on  
247 the SOA mass collected on the filter. The normalized result was defined as the mass  
248 absorption coefficient (MAC,  $m^2 g^{-1}$ ), calculated using Eq. R2:

$$MAC_{\lambda} = \frac{Abs_{\lambda}}{M} \quad (R2)$$

249 where,  $M$  ( $\mu g m^{-3}$ ) represents the concentration of methanol-soluble organic carbon.

## 250 **3 Result and Discussion**

### 251 **3.1 SOA formation**

252 In order to investigate the effect of  $NH_3$  and  $NO_x$  on SOA formation from toluene  
253 photooxidation, a control test was carried out. SOA yield ( $Y$ ) is defined as  $Y =$   
254  $\Delta M_0 / \Delta HC$ , where  $\Delta M_0$  is the produced organic aerosol mass concentration ( $\mu g m^{-3}$ ),  
255 and  $\Delta HC$  is the mass concentration of reacted toluene ( $\mu g m^{-3}$ ). The evolution of SOA  
256 mass concentrations and SOA yield at different conditions during the photooxidation  
257 process were shown in Fig. 1. Recent experiments shown that the wall loss of organic  
258 vapors to the Teflon walls should not be ignored (Zhang et al., 2014; Zhang et al.,

259 2015b), and represented a major challenge in investigating SOA formation with  
260 environmental chambers (Krechmer et al., 2020). The formation of SOA in laboratory  
261 chambers may be substantially suppressed due to losses of SOA-forming vapors to  
262 chamber walls, but this effects on SOA formation have not yet been quantitatively  
263 established. However, the particle wall loss rates were detected at the end of the  
264 chamber experiment after the UV-lamps were turned off, and the mass concentration  
265 was corrected with the same way of Jiang et al. (2020) and Pathak et al. (2007). After  
266 the wall loss correction, the particle mass concentration was almost constant, the  
267 different wall loss effect caused by gaseous oxidation products formed in the different  
268 experiment conditions was considered remedied. Interestingly, wall loss is increased  
269 66% and 205% in Exp.2 (in the presence of NH<sub>3</sub>) and Exp.3 (in the mixed condition of  
270 NH<sub>3</sub> and NO<sub>x</sub>), respectively, when compared with the experiments with no NH<sub>3</sub> (Exp.1  
271 and 4). The larger particle wall loss in the presence of NH<sub>3</sub> could be explained by  
272 increasing condensation process of oxidized organic vapors onto the Teflon chamber  
273 wall via oligomerization (for dicarbonyls) and ionic dissociation/acid-base reaction (for  
274 organic acids). There was a noticeable increase in the SOA mass concentration in the  
275 presence of NH<sub>3</sub>, which was consistent with previous studies (Qi et al., 2020;Chu et al.,  
276 2016). The mass concentration of SOA increased from  $637 \pm 14.6 \mu\text{g m}^{-3}$  without NH<sub>3</sub>  
277 to a maximum of  $867 \pm 12.7 \mu\text{g m}^{-3}$  with 200 ppb NH<sub>3</sub>. Previous studies attributed the  
278 enhancement of SOA to the formation of NOA from acid-base reactions between  
279 NH<sub>3</sub>/NH<sub>4</sub><sup>+</sup> and carboxyl groups, or Maillard reactions of NH<sub>3</sub>/NH<sub>4</sub><sup>+</sup> with carbonyl  
280 functional groups (Noziere et al., 2009;Ortiz-Montalvo et al., 2014;Liu et al., 2015;Qi

281 et al., 2020). In contrast, SOA concentrations were lower in the presence of NO<sub>x</sub>, and  
282 the maximum mass concentration of toluene SOA was only  $452 \pm 18.9 \mu\text{g m}^{-3}$  with 63  
283 ppb initial NO<sub>x</sub>. The branching of RO<sub>2</sub> loss among different pathways has an important  
284 influence on the products distribution and SOA formation. The fate of RO<sub>2</sub> mainly  
285 depends on the concentrations of NO<sub>x</sub> (Zhao et al., 2018;Liu et al., 2019a;Xu et al.,  
286 2020). Numerous studies have shown that, instead of RO<sub>2</sub> reacting with RO<sub>2</sub>/HO<sub>2</sub>, NO  
287 would react with RO<sub>2</sub> to form the RO intermediate and produces more oxidation  
288 products with higher volatilities through fragmentation in the presence of NO<sub>x</sub> (Zhao  
289 et al., 2018;Liu et al., 2019a;Xu et al., 2020). Highly volatile compounds cannot readily  
290 partition into the particle-phase, so this substantially suppresses the formation of SOA.

291 The NO<sub>x</sub> and NH<sub>3</sub> had opposite effects on toluene SOA formation in this study.  
292 Interestingly, however, the highest SOA mass concentration ( $1020 \pm 10.6 \mu\text{g m}^{-3}$ )  
293 occurred in the presence of both NO<sub>x</sub> and NH<sub>3</sub>, which was nearly 1.6 times higher than  
294 that observed with no NO<sub>x</sub> or NH<sub>3</sub>. Although inorganic aerosol was formed from the  
295 interaction of NH<sub>3</sub> and NO<sub>x</sub> in the chamber, the upper limit of the inorganic matter only  
296 account for 6.6% of the total mass of particulate matter (Table S1) in the NH<sub>3</sub> + NO<sub>x</sub>  
297 experiment. Therefore, it was not the main cause of the increase in particulate matter.  
298 Therefore, together NH<sub>3</sub> and NO<sub>x</sub> had a synergistic effect on SOA formation because  
299 their combined effect on SOA formation was greater than the sum of their separate  
300 effects. Qi et al. (2020) observed the promotion of NH<sub>3</sub> on toluene SOA formation was  
301 more obviously under high NO<sub>x</sub> concentration, SOA yield increased 3.7% and 4.6%  
302 for 70 ppb and 160 ppb initial NO<sub>x</sub> concentration, respectively, when 200 ppb NH<sub>3</sub> was

303 added into the chamber. Li et al. (2018) showed that the presence  $\text{NH}_3$  can promote the  
304 particle size growth of SOA; at the same time, this particle growth rate was higher under  
305 low VOC/NO<sub>x</sub> (or high NO<sub>x</sub>) conditions. All in all, the joint effect of multiple  
306 environmental factors on SOA formation is not the simple summation of the influences  
307 of various factors on SOA formation. This may at least partly explain why predictions  
308 of SOA concentrations in large-scale atmospheric models, which typically describe  
309 SOA formation from data derived from chamber experiments, are frequently lower than  
310 field observations (Volkamer et al., 2006).

### 311 **3.2 SOA chemical composition**

312 The traditional SOA formation mechanism is based on the chemical compositions  
313 obtained through off-line detection of the chemical composition of SOA (Jang et al.,  
314 2002;Liu et al., 2019a;Xu et al., 2020). SOA is continually evolving in the atmosphere  
315 and the ageing process of SOA co-occurs with its formation process, resulting in the  
316 transformation of SOA chemical composition continuously proceeding during the  
317 photooxidation process, but little attention has been paid to the evolution of SOA  
318 chemical composition in previous studies. Therefore, the AMS was used for on-line  
319 measurement of the SOA chemical composition and how the chemical composition  
320 evolved in the photooxidation process would be discussed in this section below.

321 Chemical composition of SOA is very complex. The average carbon oxidation  
322 state ( $\text{OS}_C$ ) has been shown to be an ideal conceptual framework to describe changes  
323 in the degree of oxidation undergone by SOA (Kroll et al., 2011), and has been widely



324 applied in field and laboratory studies (Chen et al., 2018;Mandariya et al., 2019).  
325 Average  $OS_C$  calculation was shown in Supporting Information. Fig. 2 shows the  
326 changes in the  $OS_C$  of toluene SOA formed in different experiments. Notably, toluene  
327 SOA  $OS_C$  values was in the range between -0.5 and 0, which is consistent with that of  
328 semi-volatile oxygenated organic aerosols (SV-OOA). However, the different  $OS_C$   
329 values and the change trends observed for the toluene SOA formed in different  
330 conditions (with and without  $NH_3/NO_x$ ) in Fig. 2 indicated that there was a  
331 photooxidation mechanism active during SOA formation, which ultimately changed the  
332 SOA chemical compositions.

333 The  $OS_C$  increased over time for all SOAs that were formed in the absence of  $NH_3$ .  
334 There are several possible reasons for the increasing trend of  $OS_C$  values. Firstly, a  
335 dynamic equilibrium of semi-volatile vapors may have been achieved between the  
336 particle-phase and gas-phase during the earlier toluene oxidation process. The increase  
337 of SOA led to a reduction in the concentration of gas-phase semi-volatile organic  
338 products. A decreasing concentration of gas-phase semi-volatile organic compound  
339 products would suppress their transformation from gas-phase to particulate-phase.  
340 More lower volatility gas-phase oxidation products with higher  $OS_C$  values would then  
341 be shifted to the particle phase, which would be responsible for the continuing increase  
342 of SOA and its  $OS_C$ . Secondly, the formed SOA could have further been oxidized by  
343 OH radical through heterogeneous reactions (Kourtchev et al., 2015;Liu et al., 2019b).  
344 This could be the main reason for the increase in the  $OS_C$  when the SOA concentration  
345 was no longer increasing. Finally, as pointed by Malecha and Nizkorodov (2016), even

346 if there was no OH radical in the chamber, the photodegradation of SOA can produce  
347 small oxygenated volatile organic compounds (e.g. acetaldehyde  $OS_C = -1$ , and acetone  
348  $OS_C \approx -1.3$ ) under UV light irradiation. The photoproduction of OVOCs from SOA had  
349 a lower  $OS_C$  value than that of SOA. Although the loss of SOA through  
350 photodegradation is small, the  $OS_C$  value of SOA still had increased to a certain extent  
351 (Malecha and Nizkorodov, 2016).

352 The fact that additional photochemical processing results in the dynamic evolution  
353 of the  $OS_C$  over time has been demonstrated in both field and laboratory experiments  
354 (Jimenez et al., 2009). The atmospheric oxidation of OA tends towards higher  $OS_C$   
355 regardless of the original OA source (Herndon et al., 2008). However, when  $NH_3$  was  
356 present, the  $OS_C$  of total SOA went almost unchanged for the whole photooxidation  
357 period. Carboxyl and carbonyl are the main oxygen-containing functional groups  
358 responsible for the toluene photooxidation production (Ji et al., 2017). An organic  
359 ammonium salt with four H atoms can offset an increase in  $OS_C$  value caused by the  
360 formation of organic acids/carboxy group with two O atoms through acid-base reactions  
361 (Kuwata and Martin, 2012; Liu et al., 2015). Or  $NH_3/NH_4^+$  may react with carbonyl  
362 functional groups through Maillard reactions, consuming the oxygen in the carbonyl  
363 group and leading to the formation of species with covalent carbon-nitrogen bonds (Lee  
364 et al., 2013; Zhang et al., 2015a; Qi et al., 2020). Xu et al. (2018) showed that imidazole  
365 compounds ( $OS_C \approx -1.3$ ) generated through heterogeneous reaction between  $NH_3$  and  
366 carbonyl compounds might contribute to the decrease in the  $OS_C$  of SOA. It is clear that  
367 an increase in  $OS_C$  caused by the formation of oxygen-containing functional groups

368 (e.g., carboxyl, carbonyl, etc.) would be counteracted through acid-base reactions or  
369 Maillard reactions in the presence of  $\text{NH}_3$ . After 60 min of UV light irradiation, there  
370 was no more SOA formation; however, the  $\text{OS}_C$  did decrease slightly in Exp.2 and 3,  
371 illustrating that the  $\text{NH}_3$  could continue to react with SOA through heterogeneous  
372 processes. Huang et al. (2016) also pointed out that the portion of semi-volatile products  
373 with low  $\text{OS}_C$  formed at the later stage of photooxidation also contributed to the  
374 decreased  $\text{OS}_C$ .

375 The  $\text{OS}_C$  of the toluene SOA formed with  $\text{NO}_x$  was lower than that formed in the  
376 absence of  $\text{NO}_x$ , no matter whether  $\text{NH}_3$  was present in the chamber or not. This  
377 indicated that an increased  $\text{NO}_x$  concentration benefits the formation high volatility  
378 oxidation products with lower  $\text{OS}_C$  values (Kroll et al., 2011; Jimenez et al., 2009).  
379 However, the relationships between  $\text{OS}_C$  and SOA mass concentration with and without  
380  $\text{NH}_3$  were the opposite of each other. Predictably, the SOA formation mechanism in the  
381 presence of  $\text{NO}_x$  is different from that with  $\text{NO}_x + \text{NH}_3$ . In the absence of  $\text{NH}_3$ , the RO  
382 intermediate, which is easily fragmented to produce relatively high-volatility  
383 compounds, was the dominant product of the  $\text{NO}_x + \text{RO}_2$  reaction (Zhao et al., 2018; Liu  
384 et al., 2019a; Xu et al., 2020). Highly volatile compounds cannot readily precipitate into  
385 the particle-phase, which subsequently results in a lower SOA yield in the presence of  
386  $\text{NO}_x$  (Yang et al., 2020). Thereby, both  $\text{OS}_C$  and the SOA mass concentration were  
387 lower when 60 ppb  $\text{NO}_x$  was added into the chamber. However, when both  $\text{NO}_x$  and  
388  $\text{NH}_3$  were present, the toluene derived SOA had the lowest  $\text{OS}_C$  value, but the highest  
389 mass concentration. This result suggested that although  $\text{NO}_x$  promotes the formation

390 of higher volatility compounds. These higher volatility compounds (e.g. glyoxal) can  
391 react with  $\text{NH}_3$  and precipitate into the particle-phase, which could contribute to the  
392 increase in SOA formation. Huffman et al. (2009) observed that aerosol volatility was  
393 inversely correlated with the extent of oxidation of OA components. The low value of  
394  $\text{OS}_C$  in the presence of  $\text{NO}_x$  indicated that  $\text{NO}_x$  would promote the formation of the  
395 relatively high-volatility compounds. However, the lower  $\text{OS}_C$  value in the presence of  
396  $\text{NH}_3$  indicated that the high-volatility compounds would promote partitioning into the  
397 particle-phase when reacting with  $\text{NH}_3$ .

398 Fragments derived from the AMS data have also been widely used to explore the  
399 bulk compositions and properties of SOA (Ng et al., 2010; Ng et al., 2017). The  $m/z$  43  
400 (f43) frequency was dominated by ion  $\text{C}_2\text{H}_3\text{O}^+$ , which is the tracer for organic  
401 compounds with alcohol and carbonyl functional groups (Alfarra et al., 2006).  
402 Meanwhile, the  $m/z$  44 (f44) signal was dominated by  $\text{CO}_2^+$  ions, which is the tracer  
403 for organic compounds with carboxyl functional groups and indicator of highly  
404 oxygenated organic aerosols (Ng et al., 2010). Here, we use the approach of Ng et al.  
405 (2010) by plotting the fractions of the total organic signal at  $m/z$  43 vs.  $m/z$  44 (f43 vs.  
406 f44). The change of f43 vs. f44, which has an inflection point during the photooxidation  
407 process, is shown in Fig. 3 and Fig. S3. In our study, the change before the inflection  
408 point was defined as the formation stage, and the linear fit of f43 vs. f44 for the  
409 formation stage is shown by the dashed lines. The change in f43 vs. f44 after the  
410 inflection point was defined as the stable stage, and the linear fit of f43 vs. f44 in this  
411 stage is shown by the solid lines. The formation and stable stages of the f43 vs. f44

412 relationship during the experiment are discussed separately here.

413 In the stable stage, the increase in f44 and decrease in f43 with increasing OH  
414 exposure indicated that the carbonyl groups in toluene SOA were oxidized to carboxyl  
415 groups by the ageing process. For the experiments without NH<sub>3</sub> and NO<sub>x</sub>, the slope  
416 ratio of f43 vs. f44 was -3.9. When there was 60 ppb initial NO<sub>x</sub>, the f43 was almost  
417 stable while the f44 increased with the oxidation process. There was a lower slope ratio  
418 of f43 vs. f44, indicating that organic compounds with more alcohol and carbonyl  
419 functional groups had formed in the presence of NO<sub>x</sub>. But for the experiments with 200  
420 ppb initial NH<sub>3</sub>, the slope ratios of f43 vs. f44 were only -1.1 and -1.3 in the presence  
421 and absence of NO<sub>x</sub>, respectively. According to the above results, we can see that more  
422 carbonyl groups are consumed as carboxyl groups are formed in the presence of NH<sub>3</sub>.  
423 The carbonyls can be oxidized to organic acids (Kawamura and Bikkina, 2016), but  
424 extra-consumed carbonyls can be nucleophilically attacked by NH<sub>3</sub>/NH<sub>4</sub><sup>+</sup> to form  
425 nitrogen-heterocyclic compounds, e.g., imidazole (Grace et al., 2019; Lian et al., 2020).  
426 Meanwhile, the peak f44 value decreased from 0.13 to 0.10 when NH<sub>3</sub> was added into  
427 the chamber. This suggested that the heterogeneous reaction of NH<sub>3</sub>/NH<sub>4</sub><sup>+</sup> could  
428 promote the consumption of particle-phase carbonyl groups (Xu et al., 2018), and must  
429 inhibit the formation of carboxyl groups in the SOA ageing process. According to the  
430 changing trend of SOA concentration over time, the photooxidation process was  
431 divided into formation stage and stable stage. As shown in Fig. 1, the first half hour of  
432 photooxidation when SOA concentration increased linearly with time was defined as  
433 SOA formation stage. After 60 min of photooxidation, SOA concentration was not

434 changed with reaction time, and it was defined as stable stage. The differences in spectra  
435 of toluene SOA in the formation stage and stable stage are shown in Fig. 4. A lower  
436 signal intensity variation of  $\text{CO}_2^+$  in the presence of  $\text{NH}_3$  also illustrated that  $\text{NH}_3$  would  
437 inhibit heterogeneous reactions that form carboxyl groups.

438 In the formation stage, the slope ratios of f43 vs. f44 were almost the same for both  
439 experiments without  $\text{NO}_x$ . It can thus be seen that the presence or absence of  $\text{NH}_3$  does  
440 not affect the change trend of f43 vs. f44 in the SOA formation stage. Therefore, the  
441 gas-phase homogeneous reaction of  $\text{NH}_3$  on SOA formation is not important. Clearly,  
442 the particle-phase heterogeneous reaction was the main reaction pathway by which  $\text{NH}_3$   
443 participated in the photooxidation process and toluene SOA formation. However,  
444 negative correlations were observed between f43 and f44 in the presence of  $\text{NO}_x$ . Based  
445 on this, we concluded that  $\text{NO}_x$  not only affects the SOA formation through the particle-  
446 phase heterogeneous reactions, but also through gas-phase homogeneous reactions.

### 447 **3.3 PMF results**

448 A temporal evaluation of the toluene SOA chemical composition during  
449 photooxidation is vital to the analysis of the NOA formation mechanism in the presence  
450 of  $\text{NH}_3$  and/or  $\text{NO}_x$ . Therefore, this study further compared the chemical properties of  
451 the SOA generated under different experimental conditions by applying a PMF analysis  
452 to the HR-ToF-AMS data (Chen et al., 2019). A summary of the PMF results is  
453 presented in Fig. S4-S7. For the toluene OH-photooxidation experiments with  $\text{NH}_3$   
454 and/or  $\text{NO}_x$  presence, two factors were identified from the PMF analysis in the same

455 way of Chen et al. (2019). The H/C, O/C, and N/C values of these two factors are shown  
456 in Fig. 5. The factor with higher N/C values was defined as high-nitrogen OA (Hi-NOA).  
457 In contrast, the factor with lower N/C values was defined as low-nitrogen OA (Lo-NOA).  
458 Fig. 6 exhibits the evolution of Hi-NOA and Lo-NOA during the photooxidation  
459 process as resolved from the PMF analysis of different initial NO<sub>x</sub>/NH<sub>3</sub> concentrations.  
460 While similar evolutionary trends were observed under different conditions, the relative  
461 intensities and the chemical compositions of these two factors in each experiment were  
462 not consistent.

463 For the toluene SOA formed under NH<sub>3</sub> conditions, both Lo-NOA and Hi-NOA  
464 had similar O/C values, which were fully oxygenated with an average of  $0.74 \pm 0.04$   
465 (Fig. 5a). These O/C values were comparable to the low-volatility oxygenated organic  
466 aerosols (LV-OOA) with an O/C value ranging from 0.6 to 1 (Jimenez et al., 2009). The  
467 main difference between these two OA sources was the N/C ratio. The N/C ratio of Hi-  
468 NOA (N/C = 0.032) was about three times higher than that of Lo-NOA (N/C = 0.010)  
469 (Fig. 5a). The evolution of these two OA sources during the photooxidation process is  
470 shown in Fig. 6a. The components of toluene SOA were mostly Lo-NOA during the  
471 initial phase of SOA formation, but Hi-NOA toluene SOA started forming after 10  
472 minutes and continued to increase. The Lo-NOA reached the maximum mass  
473 concentration after 30 min of the photooxidation, and then decreased. Such a decline  
474 trend of Lo-NOA at longer reaction times reflected the conversion of Lo-NOA into  
475 something else in the particle-phase. As the Lo-NOA decreased, the mass concentration  
476 of Hi-NOA gradually increased. Thus, the Hi-NOA should be derived from the

477 heterogeneous reaction of Lo-NOA with  $\text{NH}_3/\text{NH}_4^+$ . At the same time, it was proved  
478 that the formation pathway of Hi-NOA was not through reaction of  $\text{NH}_3$  with later-  
479 generation gas-phase products in the homogeneous gas phase. With the gradual  
480 replacement of Lo-NOA by Hi-NOA, the ratio of  $[\text{Hi-NOA}]/[\text{Lo-NOA}]$  stabilized at  
481 5~6.

482 For the toluene SOA formed under  $\text{NO}_x$  conditions, there was not a large  
483 difference between the N/C ratios of Hi-NOA (N/C = 0.019) and Lo-NOA (N/C = 0.014)  
484 (Fig. 5c). At the end of the  $\text{NO}_x$  experiment, the ratio of  $[\text{Hi-NOA}]/[\text{Lo-NOA}]$  was only  
485 3:2 (Fig. 6c). It follows that the contribution of the heterogeneous  $\text{NO}_x$  reaction to the  
486 N/C ratio of toluene SOA was not obvious. Therefore, the formation of NOA in the  
487 presence of  $\text{NO}_x$  mainly occurred through gas-phase homogeneous reactions, which  
488 was consistent with the results in section 3.3.

489 The changing trend of N/C with time in the presence of  $\text{NH}_3$  was different to that  
490 with  $\text{NO}_x$  present. The evolutions of the N/C of SOA in different experiments are  
491 shown in Fig. 7. In the presence of  $\text{NH}_3$ , the N/C value gradually increased throughout  
492 the photooxidation process. The increased N/C value in the photooxidation process was  
493 attributed to the heterogeneous  $\text{NH}_3$  reaction with SOA. But in the presence of  $\text{NO}_x$ ,  
494 the N/C increased rapidly to its maximum value where it was stable for the rest of the  
495 reaction. This could mean that the heterogeneous reaction of toluene SOA with  $\text{NO}_x$  to  
496 form NOA was not as important as the gas-phase homogeneous reaction.



497 When both NO<sub>x</sub> and NH<sub>3</sub> were added into the chamber, the N/C ratios of Hi-NOA  
498 and Lo-NOA were 0.062 and 0.029, respectively (Fig. 5b). The N/C ratio of Hi-NOA,  
499 which was comparable to the recently isolated nitrogen-enriched OA value (0.053)  
500 observed by Sun et al. (2011), was much higher than that observed in the experiments  
501 with only NH<sub>3</sub> or NO<sub>x</sub>. It was even higher than the sum of the N/C ratios from both  
502 Exp. 2 with NH<sub>3</sub> and Exp. 4 with NO<sub>x</sub>. In order to calculate the relative contributions  
503 of NH<sub>3</sub> and NO<sub>x</sub> to N/C, it was assumed that the effects of NH<sub>3</sub> or NO<sub>x</sub> on the N/C  
504 ratio in the Hi-NOA and Lo-NOA factors did not change among different experimental  
505 conditions. For Lo-NOA, the contributions of NH<sub>3</sub> and NO<sub>x</sub> to the N/C value were  
506 0.0126 and 0.0164, and their relative intensities were 43% and 57%, respectively. While  
507 for the Hi-NOA, the contributions of NH<sub>3</sub> and NO<sub>x</sub> to the N/C values were 0.0404 and  
508 0.0216, and their relative intensities were 65% and 35%, respectively. For the  
509 experiment with both NH<sub>3</sub> and NO<sub>x</sub>, the contribution of NH<sub>3</sub> to N/C was higher by 26%,  
510 and the contribution of NO<sub>x</sub> to N/C was higher by 17% compared to the experiments  
511 with single pollutants. The co-existence of NH<sub>3</sub> and NO<sub>x</sub> further enhanced the N/C  
512 value of toluene SOA, indicating that a synergetic interaction between NH<sub>3</sub> and NO<sub>x</sub>  
513 further enhanced organic nitrogen formation.

### 514 **3.4 Optical absorption**

515 The optical characteristics of toluene SOA formed from different NH<sub>3</sub> and NO<sub>x</sub>  
516 conditions were investigated. The MAC of toluene derived SOA detected over the range  
517 of 230–600 nm is displayed in Fig. 8. Over the entire UV detection range, an increase

518 in light absorption was observed when the toluene SOA formed in the presence of NOx  
519 or NH<sub>3</sub>.

520 By looking at Fig. 8 in detail, one can see that the MAC of toluene SOA formed  
521 with (red line) and without (black line) NH<sub>3</sub> overlapped at 250 nm, but when the UV  
522 wavelength exceeded 250 nm the MAC of the toluene SOA formed in the presence of  
523 NH<sub>3</sub> was higher. The red line reflects an obvious characteristic absorption peak at  
524 270~280 nm, which was mainly due to the absorption of the  $n \rightarrow \pi^*$  electronic  
525 transitions. The imidazole compounds were formed through the Maillard reactions  
526 between NH<sub>3</sub>/NH<sub>4</sub><sup>+</sup> with carbonyl functional groups (Zhang et al., 2015a). The C=N  
527 double bonds in the organonitrogen imidazole compounds can act as effective  
528 chromophores since both  $\pi \rightarrow \pi^*$  and  $n \rightarrow \pi^*$  transitions are chromatically active  
529 (Nguyen et al., 2013). The UV/visible spectrum of imine and pyrrole show broad bands  
530 at 270 nm (NIST, 2020), which was consistent with the UV absorption peak of the  
531  $n \rightarrow \pi^*$  band observed here. According to the AMS results, carbonyl was the main  
532 functional group of toluene SOA. The emergence of absorption peaks at 270~280 nm  
533 demonstrated that some organonitrogen imidazole compounds (e.g. imines and pyrrole)  
534 were formed through the heterogeneous reaction of toluene with NH<sub>3</sub>. Meanwhile, the  
535 high-molecular weight nitrogen-containing organic species might have formed through  
536 Maillard reactions in the particle-phase (Wang et al., 2010). This was also a reason for  
537 the increase in SOA mass concentration in the presence of NH<sub>3</sub>.

538 The green line in Fig. 8 represents the MAC value of toluene-derived SOA in the  
539 presence of NOx, which was also higher than the black line (control) throughout the

540 UV detection range. When compared with the red line, the green line had no obvious  
541 characteristic peak at 280 nm, but it had higher absorbance in the range between 240  
542 and 280 nm. This indicated that both NO<sub>x</sub> and NH<sub>3</sub> increased the absorbance of toluene  
543 SOA, while the chromophores generated from the reactions between toluene-derived  
544 SOA with either NH<sub>3</sub> or NO<sub>x</sub> did not behave in the same way.

545 The blue line in Fig. 8 represents the absorbance of toluene SOA formed in the  
546 presence of both NO<sub>x</sub> and NH<sub>3</sub>. The MAC of toluene SOA formed in the presence of  
547 both NO<sub>x</sub> and NH<sub>3</sub> was higher than the toluene SOA formed in the presence of either  
548 NH<sub>3</sub> or NO<sub>x</sub>. There might have been a synergetic effect between NO<sub>x</sub> and NH<sub>3</sub> on the  
549 absorbance of toluene SOA. Considering that the mass concentration of toluene SOA  
550 formed in the presence of both NH<sub>3</sub> and NO<sub>x</sub> was the highest, as described in section  
551 3.1, the co-existence of NH<sub>3</sub> and NO<sub>x</sub> may also result in the toluene SOA having  
552 stronger light absorption and atmospheric radiative forcing. We also noted a higher  
553 MAC value at 280 nm, which illustrated that the presence of NO<sub>x</sub> could promote the  
554 formation of imines and pyrrole in the photooxidation system of toluene with NH<sub>3</sub>.

## 555 **4 Conclusion**

556 Here we present the results of a study in which we characterized the mass  
557 concentrations, chemical compositions, and optical properties of SOA formed from the  
558 photooxidation of toluene under different NH<sub>3</sub> and NO<sub>x</sub> conditions concentrations.  
559 When compared with the control experiment, the SOA mass concentration data showed  
560 that the formation of toluene-derived SOA was enhanced in the presence of NH<sub>3</sub>,

561 through acid-base reactions between carboxyl groups or Maillard reactions with  
562 carbonyl compounds, but inhibited in the presence of NO<sub>x</sub>. Meanwhile, the mass  
563 concentration of toluene SOA formed in the presence of both NO<sub>x</sub> and NH<sub>3</sub> was higher  
564 than those formed under either NH<sub>3</sub> or NO<sub>x</sub> alone. This result indicated that there was  
565 a synergistic interaction between NH<sub>3</sub> and NO<sub>x</sub> that further enhanced toluene-derived  
566 SOA formation. At the same time, the lowest OS<sub>C</sub> value was obtained when both NH<sub>3</sub>  
567 and NO<sub>x</sub> were present. We concluded that highly volatile compounds, which were  
568 formed from toluene photooxidation in the presence of NO<sub>x</sub>, could react with NH<sub>3</sub> to  
569 form products with lower volatilities, and promoted the partitioning of these products  
570 into the particle-phase.

571 Synergetic effects of NH<sub>3</sub> and NO<sub>x</sub> on the formation of NOA and the optical  
572 properties of SOA were also observed in this study. The heterogeneous reaction was  
573 responsible for the formation of NOA in the presence of NH<sub>3</sub>. Meanwhile, an absorption  
574 peak at 270~280 nm, which is characteristic of imine and pyrrole, was observed. In  
575 contrast, the formation of NOA caused by NO<sub>x</sub> alone was mainly due to a gas phase  
576 homogeneous reaction.

577 In the actual atmosphere especially in Chinese urban atmosphere, NO<sub>x</sub> and NH<sub>3</sub>  
578 abundantly co-exist. Therefore, the findings presented here clearly show that the  
579 synergetic effects of NO<sub>x</sub> and NH<sub>3</sub> should not be neglected. In the meantime, our work  
580 provides a scientific basis for the consideration of synergistic emission reductions of  
581 NH<sub>3</sub> and NO<sub>x</sub> under the compound pollution conditions, which will contribute to  
582 reducing the burden of aerosols in the atmosphere. It has to be noted that the

583 concentration of reactants used for the experiments is much higher than that observed  
584 in polluted areas, the effect of NH<sub>3</sub> and NO<sub>x</sub> on the photooxidation of toluene with  
585 lower concentrations would be checked in the further study.

586

## 587 **Data availability**

588 The datasets are available upon request to the corresponding authors.

589

## 590 **Author contributions**

591 SL and GW designed the experiment. SL, DH and YW conducted the experiments. SL,  
592 DH, YW and GW performed the data interpretation. SL and GW wrote the paper. YW,  
593 SZ, CW, WD contributed to the paper with useful scientific discussions or comments.

594

## 595 **Competing interests**

596 The authors declare that they have no conflict of interest.

## 597 **Acknowledgements**

598 This work was financially supported by National Natural Science Foundation of  
599 China (Grant No. 42130704, 42005088); the China Postdoctoral Science Foundation  
600 (Grant No. 2019M661427); Fundamental Research Funds for the Central Universities,  
601 Director's Fund of Key Laboratory of Geographic Information Science (Ministry of  
602 Education), East China Normal University (Grant No. KLGIS2021C02); and ECNU  
603 Happiness Flower Program.

604 **Reference**

- 605 Alfarrá, M. R., Paulsen, D., Gysel, M., Garforth, A. A., Dommen, J., Prevot, A. S. H., Worsnop, D. R.,  
606 Baltensperger, U., and Coe, H.: A mass spectrometric study of secondary organic aerosols formed  
607 from the photooxidation of anthropogenic and biogenic precursors in a reaction chamber, *Atmos.*  
608 *Chem. Phys.*, 6, 5279-5293, DOI 10.5194/acp-6-5279-2006, 2006.
- 609 Babar, Z. B., Park, J.-H., and Lim, H.-J.: Influence of NH<sub>3</sub> on secondary organic aerosols from the  
610 ozonolysis and photooxidation of  $\alpha$ -pinene in a flow reactor, *Atmos. Environ.*, 164, 71-84,  
611 10.1016/j.atmosenv.2017.05.034, 2017.
- 612 Bates, K., Jacob, D., Li, K., Ivatt, P., Evans, M., Yan, Y., and Lin, J.: Development and evaluation of a  
613 new compact mechanism for aromatic oxidation in atmospheric models, *Atmos. Chem. Phys.*  
614 *Discuss.*, 2021, 1-34, 10.5194/acp-2021-605, 2021.
- 615 Berkemeier, T., Ammann, M., Mentel, T. F., Poschl, U., and Shiraiwa, M.: Organic nitrate contribution  
616 to new particle formation and growth in secondary organic aerosols from  $\alpha$ -pinene ozonolysis,  
617 *Environ. Sci. Technol.*, 50, 6334-6342, 10.1021/acs.est.6b00961, 2016.
- 618 Chen, C. L., Li, L. J., Tang, P., and Cocker, D. R.: SOA formation from photooxidation of naphthalene  
619 and methylnaphthalenes with m-xylene and surrogate mixtures, *Atmos. Environ.*, 180, 256-264,  
620 10.1016/j.atmosenv.2018.02.051, 2018.
- 621 Chen, T. Z., Liu, Y. C., Ma, Q. X., Chu, B. W., Zhang, P., Liu, C. G., Liu, J., and He, H.: Significant  
622 source of secondary aerosol: formation from gasoline evaporative emissions in the presence of SO<sub>2</sub>  
623 and NH<sub>3</sub>, *Atmos. Chem. Phys.*, 19, 8063-8081, 10.5194/acp-19-8063-2019, 2019.
- 624 Chen, Y., and Bond, T. C.: Light absorption by organic carbon from wood combustion, *Atmos. Chem.*  
625 *Phys.*, 10, 1773-1787, 10.5194/acp-10-1773-2010, 2010.
- 626 Chu, B. W., Zhang, X., Liu, Y. C., He, H., Sun, Y., Jiang, J. K., Li, J. H., and Hao, J. M.: Synergetic  
627 formation of secondary inorganic and organic aerosol: effect of SO<sub>2</sub> and NH<sub>3</sub> on particle formation  
628 and growth, *Atmos. Chem. Phys.*, 16, 14219-14230, 10.5194/acp-16-14219-2016, 2016.
- 629 de Foy, B., Lu, Z., and Streets, D. G.: Satellite NO<sub>2</sub> retrievals suggest China has exceeded its NOx  
630 reduction goals from the twelfth Five-Year Plan, *Sci. Rep.*, 6, 35912, 10.1038/srep35912, 2016.
- 631 Draper, D. C., Farmer, D. K., Desyaterik, Y., and Fry, J. L.: A qualitative comparison of secondary organic  
632 aerosol yields and composition from ozonolysis of monoterpenes at varying concentrations of NO<sub>2</sub>,  
633 *Atmos. Chem. Phys.*, 15, 12267-12281, 10.5194/acp-15-12267-2015, 2015.
- 634 Erisman, J. W., and Schaap, M.: The need for ammonia abatement with respect to secondary PM  
635 reductions in Europe, *Environ. Pollut.*, 129, 159-163, 10.1016/j.envpol.2003.08.042, 2004.
- 636 Ge, S., Wang, G., Zhang, S., Li, D., Xie, Y., Wu, C., Yuan, Q., Chen, J., and Zhang, H.: Abundant NH<sub>3</sub>  
637 in China enhances atmospheric HONO production by promoting the heterogeneous reaction of SO<sub>2</sub>  
638 with NO<sub>2</sub>, *Environ. Sci. Technol.*, 53, 14339-14347, 10.1021/acs.est.9b04196, 2019.
- 639 Grace, D. N., Sharp, J. R., Holappa, R. E., Lugos, E. N., Sebold, M. B., Griffith, D. R., Hendrickson, H.  
640 P., and Galloway, M. M.: Heterocyclic product formation in aqueous brown carbon systems, *ACS*  
641 *Earth Space Chem.*, 3, 2472-2481, 10.1021/acsearthspacechem.9b00235, 2019.
- 642 Herndon, S. C., Onasch, T. B., Wood, E. C., Kroll, J. H., Canagaratna, M. R., Jayne, J. T., Zavala, M. A.,  
643 Knighton, W. B., Mazzoleni, C., Dubey, M. K., Ulbrich, I. M., Jimenez, J. L., Seila, R., de Gouw, J.  
644 A., de Foy, B., Fast, J., Molina, L. T., Kolb, C. E., and Worsnop, D. R.: Correlation of secondary  
645 organic aerosol with odd oxygen in Mexico City, *Geophys. Res. Lett.*, 35, Artn L15804,  
646 10.1029/2008gl034058, 2008.
- 647 Huang, D. D., Zhang, X., Dalleska, N. F., Lignell, H., Coggon, M. M., Chan, C. M., Flagan, R. C.,  
648 Seinfeld, J. H., and Chan, C. K.: A note on the effects of inorganic seed aerosol on the oxidation  
649 state of secondary organic aerosol- $\alpha$ -Pinene ozonolysis, *J Geophys Res-Atmos*, 121, 12476-12483,  
650 10.1002/2016jd025999, 2016.

- 651 Huang, Y., Lee, S. C., Ho, K. F., Ho, S. S. H., Cao, N. Y., Cheng, Y., and Gao, Y.: Effect of ammonia on  
652 ozone-initiated formation of indoor secondary products with emissions from cleaning products,  
653 *Atmos. Environ.*, 59, 224-231, 10.1016/j.atmosenv.2012.04.059, 2012.
- 654 Huffman, J. A., Docherty, K. S., Mohr, C., Cubison, M. J., Ulbrich, I. M., Ziemann, P. J., Onasch, T. B.,  
655 and Jimenez, J. L.: Chemically-resolved volatility measurements of organic aerosol from different  
656 sources, *Environ. Sci. Technol.*, 43, 5351-5357, 10.1021/es803539d, 2009.
- 657 Jang, M., Czoschke, N. M., Lee, S., and Kamens, R. M.: Heterogeneous atmospheric aerosol production  
658 by acid-catalyzed particle-phase reactions, *Science*, 298, 814-817, 10.1126/science.1075798, 2002.
- 659 Ji, Y., Zhao, J., Terazono, H., Misawa, K., Levitt, N. P., Li, Y., Lin, Y., Peng, J., Wang, Y., Duan, L., Pan,  
660 B., Zhang, F., Feng, X., An, T., Marrero-Ortiz, W., Secret, J., Zhang, A. L., Shibuya, K., Molina,  
661 M. J., and Zhang, R.: Reassessing the atmospheric oxidation mechanism of toluene, *Proc. Natl.  
662 Acad. Sci. U. S. A.*, 114, 8169-8174, 10.1073/pnas.1705463114, 2017.
- 663 Jiang, X. T., Lv, C., You, B., Liu, Z. Y., Wang, X. F., and Du, L.: Joint impact of atmospheric SO<sub>2</sub> and  
664 NH<sub>3</sub> on the formation of nanoparticles from photo-oxidation of a typical biomass burning compound,  
665 *Environ Sci-Nano*, 7, 2532-2545, 10.1039/d0en00520g, 2020.
- 666 Jimenez, J. L., Canagaratna, M. R., Donahue, N. M., Prevot, A. S., Zhang, Q., Kroll, J. H., DeCarlo, P.  
667 F., Allan, J. D., Coe, H., Ng, N. L., Aiken, A. C., Docherty, K. S., Ulbrich, I. M., Grieshop, A. P.,  
668 Robinson, A. L., Duplissy, J., Smith, J. D., Wilson, K. R., Lanz, V. A., Hueglin, C., Sun, Y. L., Tian,  
669 J., Laaksonen, A., Raatikainen, T., Rautiainen, J., Vaattovaara, P., Ehn, M., Kulmala, M., Tomlinson,  
670 J. M., Collins, D. R., Cubison, M. J., Dunlea, E. J., Huffman, J. A., Onasch, T. B., Alfarra, M. R.,  
671 Williams, P. I., Bower, K., Kondo, Y., Schneider, J., Drewnick, F., Borrmann, S., Weimer, S.,  
672 Demerjian, K., Salcedo, D., Cottrell, L., Griffin, R., Takami, A., Miyoshi, T., Hatakeyama, S.,  
673 Shimono, A., Sun, J. Y., Zhang, Y. M., Dzepina, K., Kimmel, J. R., Sueper, D., Jayne, J. T., Herndon,  
674 S. C., Trimborn, A. M., Williams, L. R., Wood, E. C., Middlebrook, A. M., Kolb, C. E.,  
675 Baltensperger, U., and Worsnop, D. R.: Evolution of organic aerosols in the atmosphere, *Science*,  
676 326, 1525-1529, 10.1126/science.1180353, 2009.
- 677 Kawamura, K., and Bikkina, S.: A review of dicarboxylic acids and related compounds in atmospheric  
678 aerosols: Molecular distributions, sources and transformation, *Atmos. Res.*, 170, 140-160,  
679 10.1016/j.atmosres.2015.11.018, 2016.
- 680 Kourtchev, I., Doussin, J. F., Giorio, C., Mahon, B., Wilson, E. M., Maurin, N., Pangu, E., Venables, D.  
681 S., Wenger, J. C., and Kalberer, M.: Molecular composition of fresh and aged secondary organic  
682 aerosol from a mixture of biogenic volatile compounds: a high-resolution mass spectrometry study,  
683 *Atmos. Chem. Phys.*, 15, 5683-5695, 10.5194/acp-15-5683-2015, 2015.
- 684 Krechmer, J. E., Day, D. A., and Jimenez, J. L.: Always lost but never forgotten: Gas-phase wall losses  
685 are important in all teflon environmental chambers, *Environ. Sci. Technol.*, 54, 12890-12897,  
686 10.1021/acs.est.0c03381, 2020.
- 687 Kroll, J. H., Donahue, N. M., Jimenez, J. L., Kessler, S. H., Canagaratna, M. R., Wilson, K. R., Altieri,  
688 K. E., Mazzoleni, L. R., Wozniak, A. S., Bluhm, H., Mysak, E. R., Smith, J. D., Kolb, C. E., and  
689 Worsnop, D. R.: Carbon oxidation state as a metric for describing the chemistry of atmospheric  
690 organic aerosol, *Nat. Chem.*, 3, 133-139, 10.1038/nchem.948, 2011.
- 691 Kuwata, M., and Martin, S. T.: Phase of atmospheric secondary organic material affects its reactivity,  
692 *Proc. Natl. Acad. Sci. U. S. A.*, 109, 17354-17359, 10.1073/pnas.1209071109, 2012.
- 693 Laskin, A., Laskin, J., and Nizkorodov, S. A.: Chemistry of atmospheric brown carbon, *Chem. Rev.*, 115,  
694 4335-4382, 10.1021/cr5006167, 2015.
- 695 Laskin, J., Laskin, A., Roach, P. J., Slysz, G. W., Anderson, G. A., Nizkorodov, S. A., Bones, D. L., and  
696 Nguyen, L. Q.: High-resolution desorption electrospray ionization mass spectrometry for chemical  
697 characterization of organic aerosols, *Anal. Chem.*, 82, 2048-2058, 10.1021/ac902801f, 2010.
- 698 Laskin, J., Laskin, A., Nizkorodov, S. A., Roach, P., Eckert, P., Gilles, M. K., Wang, B., Lee, H. J., and  
699 Hu, Q.: Molecular selectivity of brown carbon chromophores, *Environ. Sci. Technol.*, 48, 12047-  
700 12055, 10.1021/es503432r, 2014.
- 701 Lee, A. K., Zhao, R., Li, R., Liggio, J., Li, S. M., and Abbatt, J. P.: Formation of light absorbing organo-

- 702 nitrogen species from evaporation of droplets containing glyoxal and ammonium sulfate, *Environ.*  
703 *Sci. Technol.*, 47, 12819-12826, 10.1021/es402687w, 2013.
- 704 Li, K., Chen, L., White, S. J., Yu, H., Wu, X., Gao, X., Azzi, M., and Cen, K.: Smog chamber study of  
705 the role of NH<sub>3</sub> in new particle formation from photo-oxidation of aromatic hydrocarbons, *Sci. Total*  
706 *Environ.*, 619-620, 927-937, 10.1016/j.scitotenv.2017.11.180, 2018.
- 707 Lian, X., Zhang, G., Yang, Y., Lin, Q., Fu, Y., Jiang, F., Peng, L., Hu, X., Chen, D., Wang, X., Peng, P.  
708 a., Sheng, G., and Bi, X.: Evidence for the formation of imidazole from carbonyls and reduced  
709 nitrogen species at the individual particle level in the ambient atmosphere, *Environ. Sci. Tech. Let.*,  
710 10.1021/acs.estlett.0c00722, 2020.
- 711 Liu, M., Huang, X., Song, Y., Xu, T., Wang, S., Wu, Z., Hu, M., Zhang, L., Zhang, Q., Pan, Y., Liu, X.,  
712 and Zhu, T.: Rapid SO<sub>2</sub> emission reductions significantly increase tropospheric ammonia  
713 concentrations over the North China Plain, *Atmos. Chem. Phys.*, 18, 17933-17943, 10.5194/acp-18-  
714 17933-2018, 2018.
- 715 Liu, S. J., Jia, L., Xu, Y., Tsona, N. T., Ge, S. S., and Du, L.: Photooxidation of cyclohexene in the  
716 presence of SO<sub>2</sub>: SOA yield and chemical composition, *Atmos. Chem. Phys.*, 17, 13329-13343,  
717 10.5194/acp-17-13329-2017, 2017.
- 718 Liu, S. J., Jiang, X. T., Tsona, N. T., Lv, C., and Du, L.: Effects of NO<sub>x</sub>, SO<sub>2</sub> and RH on the SOA formation  
719 from cyclohexene photooxidation, *Chemosphere*, 216, 794-804,  
720 10.1016/j.chemosphere.2018.10.180, 2019a.
- 721 Liu, S. J., Tsona, N. T., Zhang, Q., Jia, L., Xu, Y. F., and Du, L.: Influence of relative humidity on  
722 cyclohexene SOA formation from OH photooxidation, *Chemosphere*, 231, 478-486,  
723 10.1016/j.chemosphere.2019.05.131, 2019b.
- 724 Liu, S. J., Wang, Y., Wang, G., Zhang, S., Li, D., Du, L., Wu, C., Du, W., and Ge, S.: Enhancing effect  
725 of NO<sub>2</sub> on the formation of light-absorbing secondary organic aerosols from toluene photooxidation,  
726 *Sci. Total Environ.*, 794, 148714, 10.1016/j.scitotenv.2021.148714, 2021.
- 727 Liu, Y. C., Liggio, J., Staebler, R., and Li, S. M.: Reactive uptake of ammonia to secondary organic  
728 aerosols: Kinetics of organonitrogen formation, *Atmos. Chem. Phys.*, 15, 13569-13584,  
729 10.5194/acp-15-13569-2015, 2015.
- 730 Ma, P., Zhang, P., Shu, J., Yang, B., and Zhang, H.: Characterization of secondary organic aerosol from  
731 photo-oxidation of gasoline exhaust and specific sources of major components, *Environ. Pollut.*,  
732 232, 65-72, 10.1016/j.envpol.2017.09.018, 2018a.
- 733 Ma, Q., Lin, X., Yang, C., Long, B., Gai, Y., and Zhang, W.: The influences of ammonia on aerosol  
734 formation in the ozonolysis of styrene: Roles of Criegee intermediate reactions, *R. Soc. Open Sci.*,  
735 5, 172171, 10.1098/rsos.172171, 2018b.
- 736 Malecha, K. T., and Nizkorodov, S. A.: Photodegradation of secondary organic aerosol particles as a  
737 source of small, oxygenated volatile organic compounds, *Environ. Sci. Technol.*, 50, 9990-9997,  
738 10.1021/acs.est.6b02313, 2016.
- 739 Mandariya, A. K., Gupta, T., and Tripathi, S. N.: Effect of aqueous-phase processing on the formation  
740 and evolution of organic aerosol (OA) under different stages of fog life cycles, *Atmos. Environ.*,  
741 206, 60-71, 10.1016/j.atmosenv.2019.02.047, 2019.
- 742 Middlebrook, A. M., Bahreini, R., Jimenez, J. L., and Canagaratna, M. R.: Evaluation of composition-  
743 dependent collection efficiencies for the aerodyne aerosol mass spectrometer using field data,  
744 *Aerosol Sci. Tech.*, 46, 258-271, 10.1080/02786826.2011.620041, 2012.
- 745 Moise, T., Flores, J. M., and Rudich, Y.: Optical properties of secondary organic aerosols and their  
746 changes by chemical processes, *Chem. Rev.*, 115, 4400-4439, 10.1021/cr5005259, 2015.
- 747 Na, K., Song, C., Switzer, C., and Cocker, D. R.: Effect of ammonia on secondary organic aerosol  
748 formation from  $\alpha$ -pinene ozonolysis in dry and humid conditions, *Environ. Sci. Technol.*, 41, 6096-  
749 6102, 10.1021/es061956y, 2007.
- 750 Ng, N. L., Chhabra, P. S., Chan, A. W. H., Surratt, J. D., Kroll, J. H., Kwan, A. J., McCabe, D. C.,



- 751 Wennberg, P. O., Sorooshian, A., Murphy, S. M., Dalleska, N. F., Flagan, R. C., and Seinfeld, J. H.:  
 752 Effect of NO<sub>x</sub> level on secondary organic aerosol (SOA) formation from the photooxidation of  
 753 terpenes, *Atmos. Chem. Phys.*, 7, 5159-5174, 10.5194/acp-7-5159-2007, 2007a.
- 754 Ng, N. L., Kroll, J. H., Chan, A. W. H., Chhabra, P. S., Flagan, R. C., and Seinfeld, J. H.: Secondary  
 755 organic aerosol formation from m-xylene, toluene, and benzene, *Atmos. Chem. Phys.*, 7, 3909-3922,  
 756 10.5194/acp-7-3909-2007, 2007b.
- 757 Ng, N. L., Canagaratna, M. R., Zhang, Q., Jimenez, J. L., Tian, J., Ulbrich, I. M., Kroll, J. H., Docherty,  
 758 K. S., Chhabra, P. S., Bahreini, R., Murphy, S. M., Seinfeld, J. H., Hildebrandt, L., Donahue, N. M.,  
 759 DeCarlo, P. F., Lanz, V. A., Prévôt, A. S. H., Dinar, E., Rudich, Y., and Worsnop, D. R.: Organic  
 760 aerosol components observed in Northern Hemispheric datasets from Aerosol Mass Spectrometry,  
 761 *Atmos. Chem. Phys.*, 10, 4625-4641, 10.5194/acp-10-4625-2010, 2010.
- 762 Ng, N. L., Brown, S. S., Archibald, A. T., Atlas, E., Cohen, R. C., Crowley, J. N., Day, D. A., Donahue,  
 763 N. M., Fry, J. L., Fuchs, H., Griffin, R. J., Guzman, M. I., Herrmann, H., Hodzic, A., Iinuma, Y.,  
 764 Jimenez, J. L., Kiendler-Scharr, A., Lee, B. H., Luecken, D. J., Mao, J., McLaren, R., Mutzel, A.,  
 765 Osthoff, H. D., Ouyang, B., Picquet-Varrault, B., Platt, U., Pye, H. O. T., Rudich, Y., Schwantes, R.  
 766 H., Shiraiwa, M., Stutz, J., Thornton, J. A., Tilgner, A., Williams, B. J., and Zaveri, R. A.: Nitrate  
 767 radicals and biogenic volatile organic compounds: Oxidation, mechanisms, and organic aerosol,  
 768 *Atmos. Chem. Phys.*, 17, 2103-2162, 10.5194/acp-17-2103-2017, 2017.
- 769 Nguyen, T. B., Laskin, A., Laskin, J., and Nizkorodov, S. A.: Brown carbon formation from  
 770 ketoaldehydes of biogenic monoterpene, *Faraday Discuss.*, 165, 473-494, 10.1039/c3fd00036b,  
 771 2013.
- 772 NIST: NIST Chemistry WebBook Standard Reference Database 69, <https://doi.org/10.18434/T4D303>,  
 773 2020.
- 774 Noziere, B., Dziedzic, P., and Cordova, A.: Products and kinetics of the liquid-phase reaction of glyoxal  
 775 catalyzed by ammonium ions (NH<sub>4</sub><sup>+</sup>), *J. Phys. Chem. A*, 113, 231-237, 10.1021/jp8078293, 2009.
- 776 Ortiz-Montalvo, D. L., Hakkinen, S. A., Schwier, A. N., Lim, Y. B., McNeill, V. F., and Turpin, B. J.:  
 777 Ammonium addition (and aerosol pH) has a dramatic impact on the volatility and yield of glyoxal  
 778 secondary organic aerosol, *Environ. Sci. Technol.*, 48, 255-262, 10.1021/es4035667, 2014.
- 779 Paciga, A. L., Riipinen, I., and Pandis, S. N.: Effect of ammonia on the volatility of organic diacids,  
 780 *Environ. Sci. Technol.*, 48, 13769-13775, 10.1021/es5037805, 2014.
- 781 Pathak, R. K., Stanier, C. O., Donahue, N. M., and Pandis, S. N.: Ozonolysis of alpha-pinene at  
 782 atmospherically relevant concentrations: Temperature dependence of aerosol mass fractions (yields),  
 783 *J. Geophys. Res.-Atmos.*, 112, Art. D03201, 10.1029/2006jd007436, 2007.
- 784 Peng, C., Yang, F., Tian, M., Shi, G., Li, L., Huang, R. J., Yao, X., Luo, B., Zhai, C., and Chen, Y.: Brown  
 785 carbon aerosol in two megacities in the Sichuan Basin of southwestern China: Light absorption  
 786 properties and implications, *Sci. Total Environ.*, 719, 137483, 10.1016/j.scitotenv.2020.137483,  
 787 2020.
- 788 Prinn, R. G., Weiss, R. F., Miller, B. R., Huang, J., Alyea, F. N., Cunnold, D. M., Fraser, P. J., Hartley, D.  
 789 E., and Simmonds, P. G.: Atmospheric trends and lifetime of CH<sub>3</sub>CCl<sub>3</sub> and global OH  
 790 concentrations, *Science*, 269, 187-192, 10.1126/science.269.5221.187, 1995.
- 791 Qi, X., Zhu, S., Zhu, C., Hu, J., Lou, S., Xu, L., Dong, J., and Cheng, P.: Smog chamber study of the  
 792 effects of NO<sub>x</sub> and NH<sub>3</sub> on the formation of secondary organic aerosols and optical properties from  
 793 photo-oxidation of toluene, *Sci. Total Environ.*, 727, 138632, 10.1016/j.scitotenv.2020.138632,  
 794 2020.
- 795 Sarrafzadeh, M., Wildt, J., Pullinen, I., Springer, M., Kleist, E., Tillmann, R., Schmitt, S. H., Wu, C.,  
 796 Mentel, T. F., Zhao, D. F., Hastie, D. R., and Kiendler-Scharr, A.: Impact of NO<sub>x</sub> and OH on  
 797 secondary organic aerosol formation from β-pinene photooxidation, *Atmos. Chem. Phys.*, 16,  
 798 11237-11248, 10.5194/acp-16-11237-2016, 2016.
- 799 Sun, Y. L., Zhang, Q., Schwab, J. J., Demerjian, K. L., Chen, W. N., Bae, M. S., Hung, H. M., Hogrefe,  
 800 O., Frank, B., Rattigan, O. V., and Lin, Y. C.: Characterization of the sources and processes of  
 801 organic and inorganic aerosols in New York city with a high-resolution time-of-flight aerosol mass

- 802           apectrometer, *Atmos. Chem. Phys.*, 11, 1581-1602, 10.5194/acp-11-1581-2011, 2011.
- 803   Surratt, J. D., Murphy, S. M., Kroll, J. H., Ng, N. L., Hildebrandt, L., Sorooshian, A., Szmigielski, R.,  
804       Vermeulen, R., Maenhaut, W., Claeys, M., Flagan, R. C., and Seinfeld, J. H.: Chemical composition  
805       of secondary organic aerosol formed from the photooxidation of isoprene, *J. Phys. Chem. A*, 110,  
806       9665-9690, 10.1021/jp061734m, 2006.
- 807   Volkamer, R., Jimenez, J. L., San Martini, F., Dzepina, K., Zhang, Q., Salcedo, D., Molina, L. T., Worsnop,  
808       D. R., and Molina, M. J.: Secondary organic aerosol formation from anthropogenic air pollution:  
809       Rapid and higher than expected, *Geophys. Res. Lett.*, 33, Artn L17811, 10.1029/2006gl026899,  
810       2006.
- 811   Vu, T. V., Shi, Z., Cheng, J., Zhang, Q., He, K., Wang, S., and Harrison, R. M.: Assessing the impact of  
812       clean air action on air quality trends in Beijing using a machine learning technique, *Atmos. Chem.*  
813       *Phys.*, 19, 11303-11314, 10.5194/acp-19-11303-2019, 2019.
- 814   Wang, G., Zhang, F., Peng, J., Duan, L., Ji, Y., Marrero-Ortiz, W., Wang, J., Li, J., Wu, C., Cao, C., Wang,  
815       Y., Zheng, J., Secret, J., Li, Y., Wang, Y., Li, H., Li, N., and Zhang, R.: Particle acidity and sulfate  
816       production during severe haze events in China cannot be reliably inferred by assuming a mixture of  
817       inorganic salts, *Atmos. Chem. Phys.*, 18, 10123-10132, 10.5194/acp-18-10123-2018, 2018a.
- 818   Wang, G. H., Zhang, R. Y., Gomez, M. E., Yang, L. X., Zamora, M. L., Hu, M., Lin, Y., Peng, J. F., Guo,  
819       S., Meng, J. J., Li, J. J., Cheng, C. L., Hu, T. F., Ren, Y. Q., Wang, Y. S., Gao, J., Cao, J. J., An, Z.  
820       S., Zhou, W. J., Li, G. H., Wang, J. Y., Tian, P. F., Marrero-Ortiz, W., Secret, J., Du, Z. F., Zheng,  
821       J., Shang, D. J., Zeng, L. M., Shao, M., Wang, W. G., Huang, Y., Wang, Y., Zhu, Y. J., Li, Y. X., Hu,  
822       J. X., Pan, B., Cai, L., Cheng, Y. T., Ji, Y. M., Zhang, F., Rosenfeld, D., Liss, P. S., Duce, R. A.,  
823       Kolb, C. E., and Molina, M. J.: Persistent sulfate formation from London Fog to Chinese haze, *Proc.*  
824       *Natl. Acad. Sci. U. S. A.*, 113, 13630-13635, 10.1073/pnas.1616540113, 2016.
- 825   Wang, R. Y., Ye, X. N., Liu, Y. X., Li, H. W., Yang, X., Chen, J. M., Gao, W., and Yin, Z.: Characteristics  
826       of atmospheric ammonia and its relationship with vehicle emissions in a megacity in China, *Atmos.*  
827       *Environ.*, 182, 97-104, 10.1016/j.atmosenv.2018.03.047, 2018b.
- 828   Wang, S. W., Zhang, Q., Martin, R. V., Philip, S., Liu, F., Li, M., Jiang, X. T., and He, K. B.: Satellite  
829       measurements oversee China's sulfur dioxide emission reductions from coal-fired power plants,  
830       *Environ. Res. Lett.*, 10, 114015, 10.1088/1748-9326/10/11/114015, 2015.
- 831   Wang, X., Gao, S., Yang, X., Chen, H., Chen, J., Zhuang, G., Surratt, J. D., Chan, M. N., and Seinfeld, J.  
832       H.: Evidence for high molecular weight nitrogen-containing organic salts in urban aerosols, *Environ.*  
833       *Sci. Technol.*, 44, 4441-4446, 10.1021/es1001117, 2010.
- 834   Wang, Y., Chen, Y., Wu, Z., Shang, D., Bian, Y., Du, Z., Schmitt, S. H., Su, R., Gkatzelis, G. I., Schlag,  
835       P., Hohaus, T., Voliotis, A., Lu, K., Zeng, L., Zhao, C., Alfarra, M. R., McFiggans, G., Wiedensohler,  
836       A., Kiendler-Scharr, A., Zhang, Y., and Hu, M.: Mutual promotion between aerosol particle liquid  
837       water and particulate nitrate enhancement leads to severe nitrate-dominated particulate matter  
838       pollution and low visibility, *Atmos. Chem. Phys.*, 20, 2161-2175, 10.5194/acp-20-2161-2020, 2020.
- 839   Wu, C., Zhang, S., Wang, G., Lv, S., Li, D., Liu, L., Li, J., Liu, S., Du, W., Meng, J., Qiao, L., Zhou, M.,  
840       Huang, C., and Wang, H.: Efficient heterogeneous formation of ammonium nitrate on the saline  
841       mineral particle surface in the atmosphere of east asia during dust storm periods, *Environ. Sci.*  
842       *Technol.*, 54, 15622-15630, 10.1021/acs.est.0c04544, 2020.
- 843   Xia, Y., Zhao, Y., and Nielsen, C. P.: Benefits of China's efforts in gaseous pollutant control indicated by  
844       the bottom-up emissions and satellite observations 2000-2014, *Atmos. Environ.*, 136, 43-53,  
845       10.1016/j.atmosenv.2016.04.013, 2016.
- 846   Xie, M., Chen, X., Hays, M. D., Lewandowski, M., Offenber, J., Kleindienst, T. E., and Holder, A. L.:  
847       Light absorption of secondary organic aerosol: Composition and contribution of nitroaromatic  
848       compounds, *Environ. Sci. Technol.*, 51, 11607-11616, 10.1021/acs.est.7b03263, 2017.
- 849   Xu, J., Huang, M. Q., Cai, S. Y., Liao, Y. M., Hu, C. J., Zhao, W. X., Gu, X. J., and Zhang, W. J.: Chemical  
850       composition and reaction mechanisms for aged p-xylene secondary organic aerosol in the presence  
851       of ammonia, *J. Chin. Chem. Soc.*, 65, 578-590, 10.1002/jccs.201700249, 2018.
- 852   Xu, L., Kollman, M. S., Song, C., Shilling, J. E., and Ng, N. L.: Effects of NO<sub>x</sub> on the volatility of

- 853 secondary organic aerosol from isoprene photooxidation, *Environ. Sci. Technol.*, 48, 2253-2262,  
854 10.1021/es404842g, 2014.
- 855 Xu, L., Moller, K. H., Crounse, J. D., Kjaergaard, H. G., and Wennberg, P. O.: New insights into the  
856 radical chemistry and product distribution in the OH-initiated oxidation of benzene, *Environ. Sci.*  
857 *Technol.*, 54, 13467-13477, 10.1021/acs.est.0c04780, 2020.
- 858 Yang, W. Y., Li, J., Wang, M., Sun, Y. L., and Wang, Z. F.: A case study of investigating secondary organic  
859 aerosol formation pathways in Beijing using an observation-based SOA box model, *Aerosol Air*  
860 *Qual. Res.*, 18, 1606-1616, 10.4209/aaqr.2017.10.0415, 2018.
- 861 Yang, Y., Vance, M., Tou, F. Y., Tiwari, A., Liu, M., and Hochella, M. F.: Nanoparticles in road dust from  
862 impervious urban surfaces: Distribution, identification, and environmental implications, *Environ*  
863 *Sci-Nano*, 3, 534-544, 10.1039/c6en00056h, 2016.
- 864 Yang, Z., Tsona, N. T., Li, J., Wang, S., Xu, L., You, B., and Du, L.: Effects of NO<sub>x</sub> and SO<sub>2</sub> on the  
865 secondary organic aerosol formation from the photooxidation of 1,3,5-trimethylbenzene: A new  
866 source of organosulfates, *Environ. Pollut.*, 264, 114742, 10.1016/j.envpol.2020.114742, 2020.
- 867 Zhang, L., Wang, Y., Feng, C., Liang, S., Liu, Y., Du, H., and Jia, N.: Understanding the industrial NO<sub>x</sub>  
868 and SO<sub>2</sub> pollutant emissions in China from sector linkage perspective, *Sci. Total Environ.*, 770,  
869 145242, 10.1016/j.scitotenv.2021.145242, 2021a.
- 870 Zhang, Q., Jimenez, J. L., Canagaratna, M. R., Ulbrich, I. M., Ng, N. L., Worsnop, D. R., and Sun, Y.:  
871 Understanding atmospheric organic aerosols via factor analysis of aerosol mass spectrometry: a  
872 review, *Anal. Bioanal. Chem.*, 401, 3045-3067, 10.1007/s00216-011-5355-y, 2011.
- 873 Zhang, R., Wang, G., Guo, S., Zamora, M. L., Ying, Q., Lin, Y., Wang, W., Hu, M., and Wang, Y.:  
874 Formation of urban fine particulate matter, *Chem. Rev.*, 115, 3803-3855,  
875 10.1021/acs.chemrev.5b00067, 2015a.
- 876 Zhang, S., Li, D., Ge, S., Liu, S., Wu, C., Wang, Y., Chen, Y., Lv, S., Wang, F., Meng, J., and Wang, G.:  
877 Rapid sulfate formation from synergetic oxidation of SO<sub>2</sub> by O<sub>3</sub> and NO<sub>2</sub> under ammonia-rich  
878 conditions: Implications for the explosive growth of atmospheric PM<sub>2.5</sub> during haze events in China,  
879 *Sci. Total Environ.*, 772, 144897, 10.1016/j.scitotenv.2020.144897, 2021b.
- 880 Zhang, X., Cappa, C. D., Jathar, S. H., McVay, R. C., Ensberg, J. J., Kleeman, M. J., and Seinfeld, J. H.:  
881 Influence of vapor wall loss in laboratory chambers on yields of secondary organic aerosol, *Proc.*  
882 *Natl. Acad. Sci. U. S. A.*, 111, 5802-5807, 10.1073/pnas.1404727111, 2014.
- 883 Zhang, X., Schwantes, R. H., McVay, R. C., Lignell, H., Coggon, M. M., Flagan, R. C., and Seinfeld, J.  
884 H.: Vapor wall deposition in Teflon chambers, *Atmos. Chem. Phys.*, 15, 4197-4214, 10.5194/acp-  
885 15-4197-2015, 2015b.
- 886 Zhao, D. F., Schmitt, S. H., Wang, M. J., Acir, I. H., Tillmann, R., Tan, Z. F., Novelli, A., Fuchs, H.,  
887 Pullinen, I., Wegener, R., Rohrer, F., Wildt, J., Kiendler-Scharr, A., Wahner, A., and Mentel, T. F.:  
888 Effects of NO<sub>x</sub> and SO<sub>2</sub> on the secondary organic aerosol formation from photooxidation of  $\alpha$ -  
889 pinene and limonene, *Atmos. Chem. Phys.*, 18, 1611-1628, 10.5194/acp-18-1611-2018, 2018.
- 890 Zou, Y., Deng, X. J., Zhu, D., Gong, D. C., Wang, H., Li, F., Tan, H. B., Deng, T., Mai, B. R., Liu, X. T.,  
891 and Wang, B. G.: Characteristics of 1 year of observational data of VOCs, NO<sub>x</sub> and O<sub>3</sub> at a suburban  
892 site in Guangzhou, China, *Atmos. Chem. Phys.*, 15, 6625-6636, 10.5194/acp-15-6625-2015, 2015.

893

894

895 **Tables**

896

897

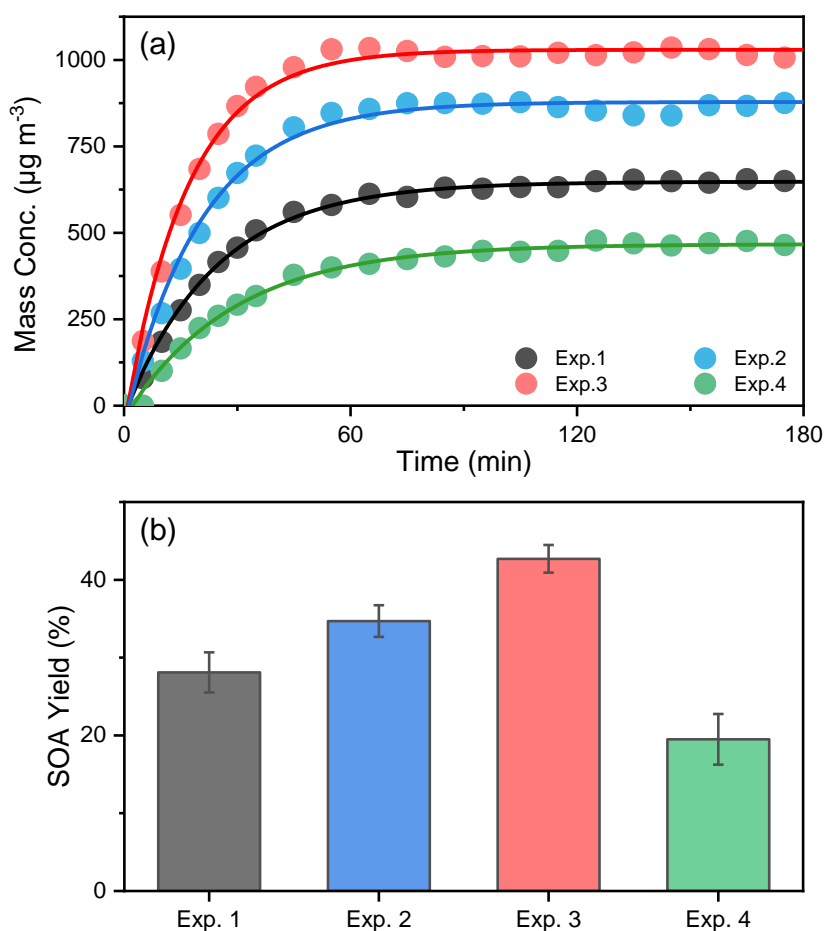
**Table 1.** Summary of experimental conditions in this study

No.	Tol <sub>0</sub> (ppb)	Δ Tol (ppb)	NH <sub>3</sub> <sup>a</sup> (ppb)	NO <sub>2</sub> (ppb)	RH (%)	SOA mass conc. <sup>b,c</sup> (μg m <sup>-3</sup> )	SOA yield <sup>b</sup> (%)
Exp.1	664.1	551.2	-	-	25 ± 1	637 ± 14.6	28.1
Exp.2	618.7	499.4	~200	-	23 ± 1	867 ± 12.7	34.7
Exp.3	620.9	526.1	~200	62	26 ± 1	1020 ± 10.6	42.7
Exp.4	645.7	539.5	-	63	25 ± 1	452 ± 18.9	19.5

898 <sup>a</sup> The concentration of NH<sub>3</sub> is estimated by the amount of NH<sub>3</sub> added and the volume of the smog  
 899 chamber. <sup>b</sup> SOA concentration and yield were calculated after taking into account the wall loss. <sup>c</sup>  
 900 The reported SOA mass concentrations was the peak values after the wall loss correction.

901

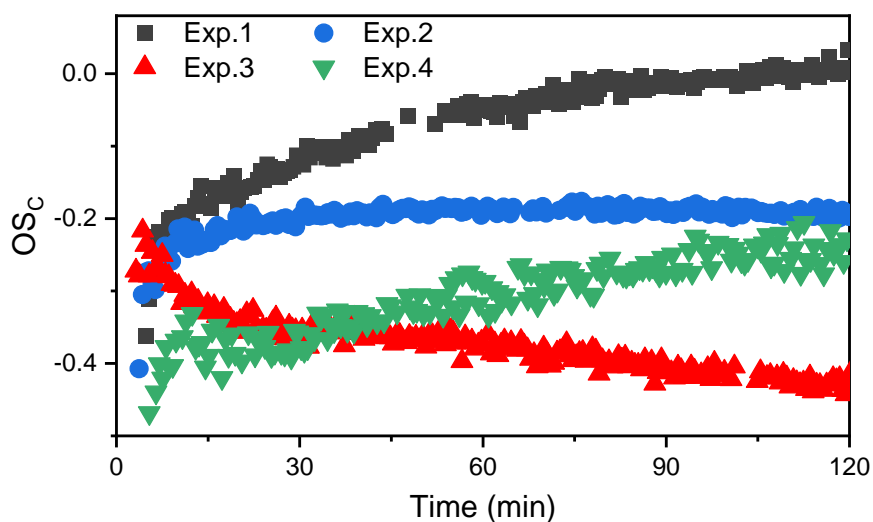
902 **Figures**



903

904

905 **Fig. 1.** The evolution of mass concentration (a) and yield (b) of toluene-derived SOA in different  
 906 experiments. All the mass concentrations were wall-loss corrected. The error bars were calculated  
 907 by the fluctuation of measured SOA concentration after the UV light was turn off at the end of  
 908 each experiment



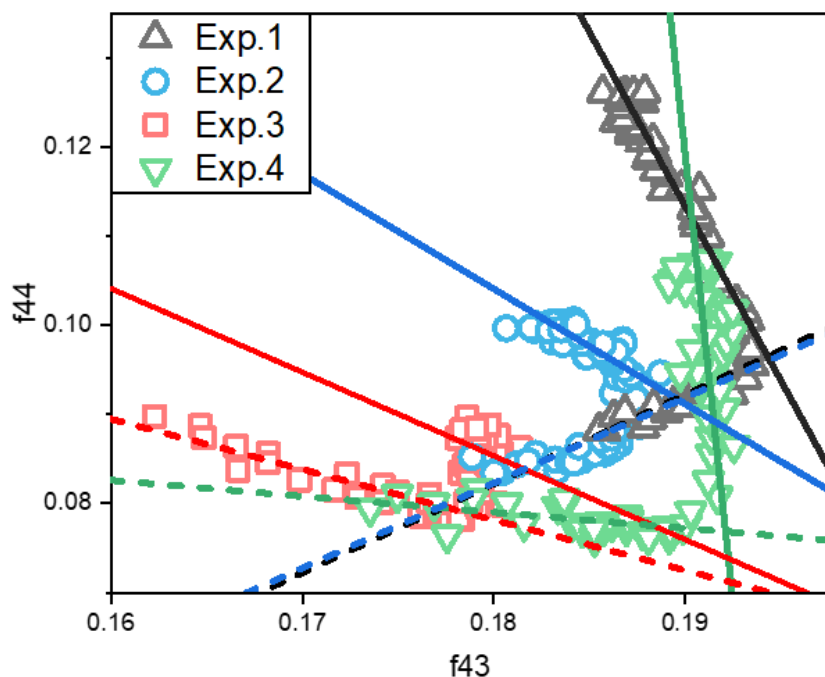
909

910 **Fig. 2.** The  $OS_C$  values for the toluene SOA formed under different  $NH_3/NO_x$  conditions.

911

912

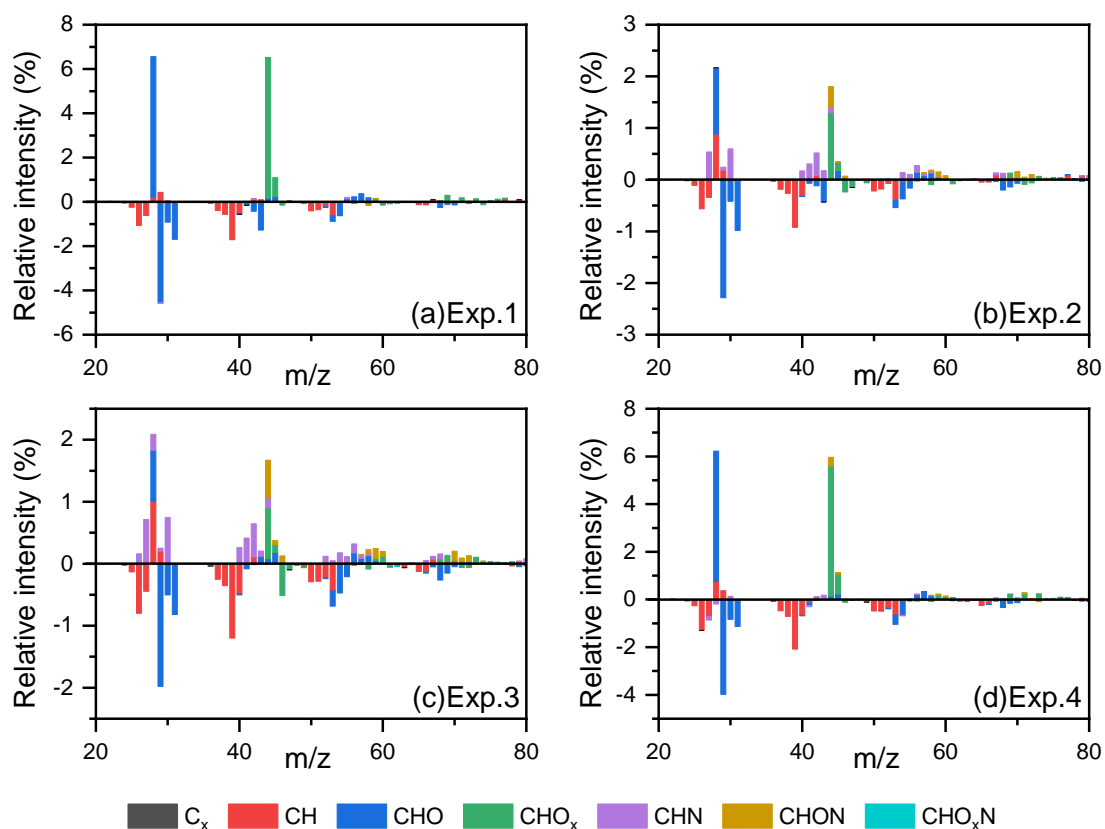
913



914

915 **Fig. 3.** The relationship between total organic signals at 43 m/z ( $f_{43}$ ) vs. 44 m/z ( $f_{44}$ ) from SOA  
 916 data during the photooxidation process. The  $f_{43}$  vs.  $f_{44}$  plots exhibited inflection points during the  
 917 photooxidation process. The dashed lines indicate the trends of  $f_{43}$  vs.  $f_{44}$  for the SOA formation  
 918 stage (before the inflection point) and the solid lines for the stable stage.

919



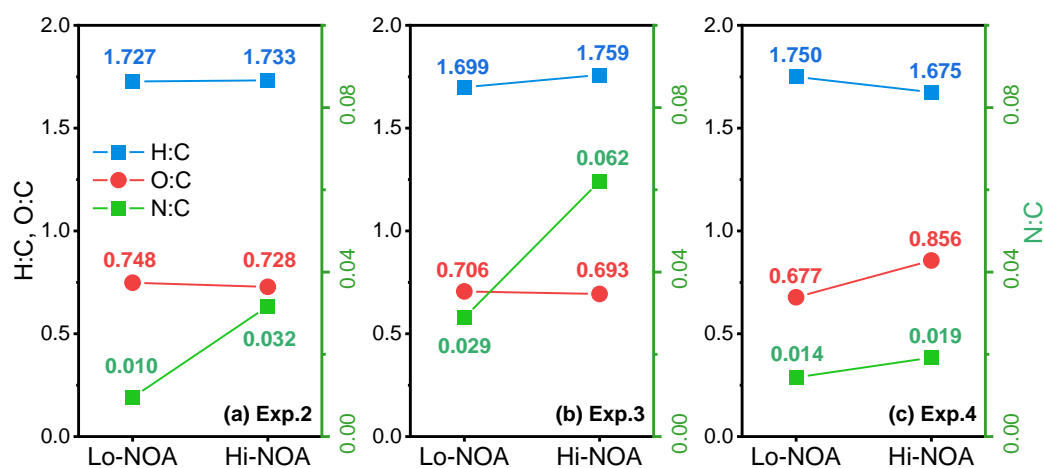
920

921 **Fig. 4.** The differential spectra of toluene SOA in the formation and stable stages. Data were taken  
 922 and analyzed at a high resolution but were summarized to a unit mass resolution for display. Only  
 923 minimal N-containing fragments could be observed in the Exp.1 without added  $\text{NH}_3$  and  $\text{NO}_x$ .

924 These N-containing fragments could be attributed to the background  $\text{NH}_3$  and  $\text{NO}_x$  in the chamber  
 925 or the systematic errors from AMS.

926

927



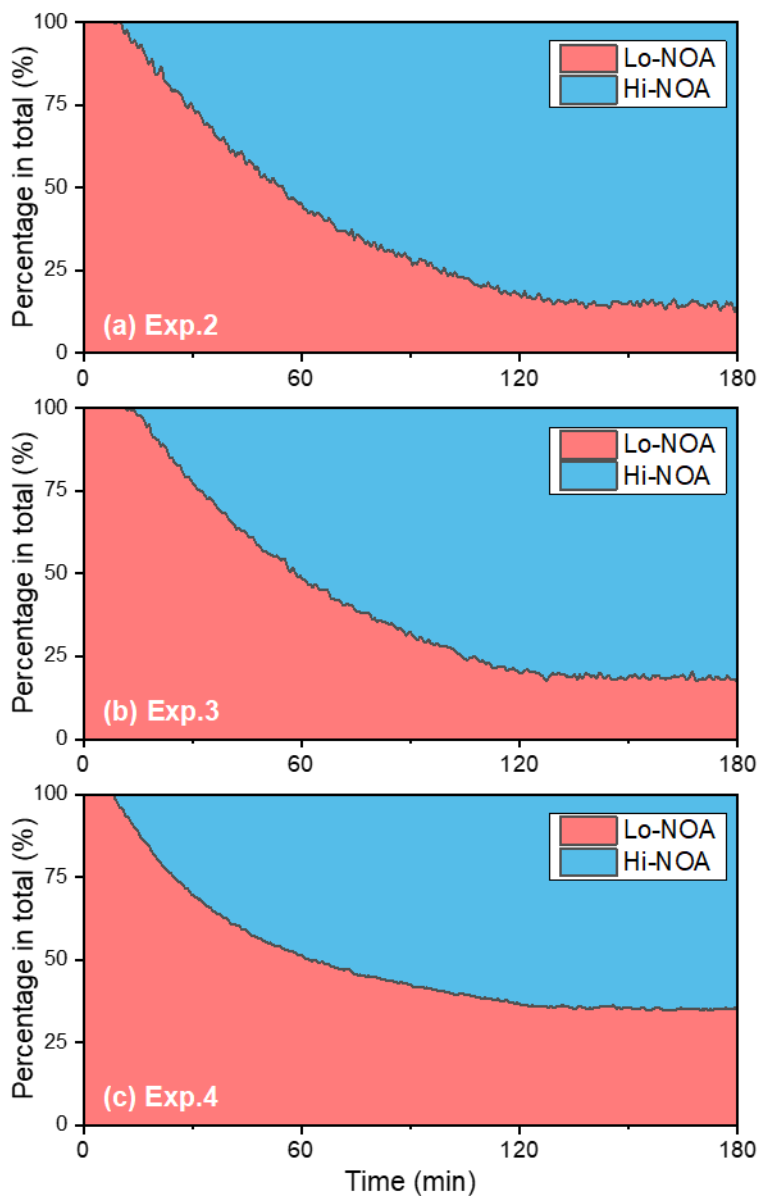
928

929 **Fig. 5.** The H/C, O/C, and N/C values of Hi-NOA and Lo-NOA for each experiment. (a) Exp. 2

930 with 200 ppb NH<sub>3</sub>, (b) Exp. 3 with 200 ppb NH<sub>3</sub> and 62 ppb NO<sub>2</sub>, and (c) Exp. 4 with 63 ppb

931 NO<sub>2</sub>.

932

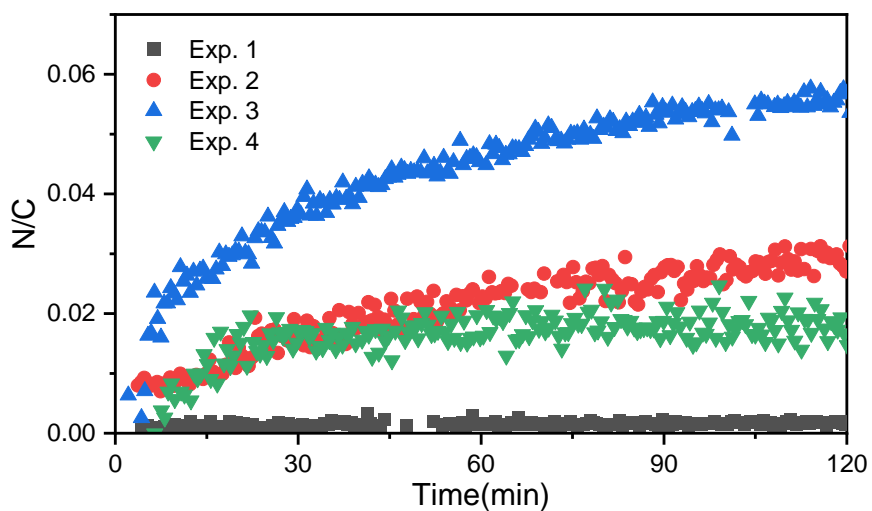


933

934 **Fig. 6.** The evolution of high-nitrogen OA (Hi-NOA) and low-nitrogen OA (Lo-NOA) during the  
 935 photooxidation process under different NO<sub>x</sub>/NH<sub>3</sub> concentrations. Hi-NOA and Lo-NOA were not  
 936 consistent among experiments. (a) Exp. 2 with 200 ppb NH<sub>3</sub>, (b) Exp. 3 with 200 ppb NH<sub>3</sub> and 62  
 937 ppb NO<sub>2</sub>, and (c) Exp. 4 with 63 ppb NO<sub>2</sub>.

938





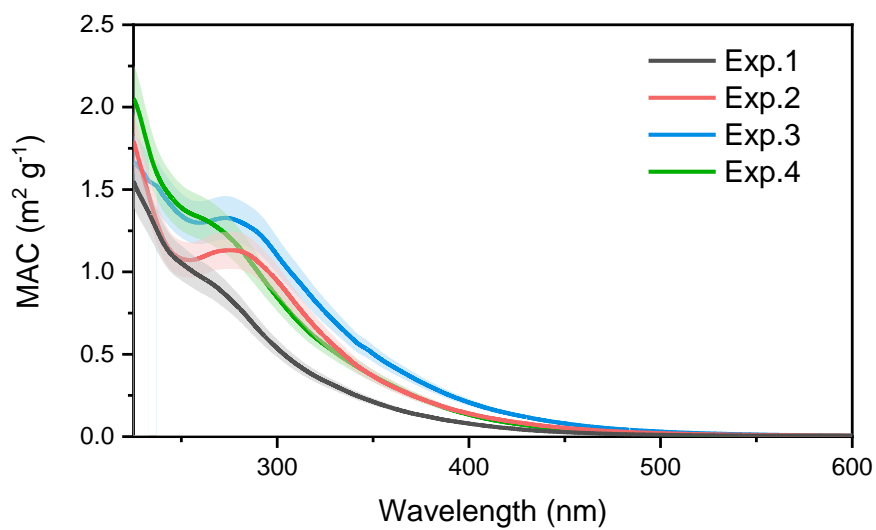
939

940 **Fig. 7.** The evolution of N/C in different experiments.

941

942

943



944

945 **Fig. 8.** The MAC over the range of 230 – 600 nm for the toluene SOA formed under different  
946 experiment conditions.

947